Available online at www.sciencedirect.com
SCIENCE DIRECT®
Comput. Methods Appl. Mech. Engrg. 192 (2003) 851–875
Computer methods in applied mechanics and engineering
www.elsevier.com/locate/cma

Non-linear strain–displacement equations exactly representing large rigid-body motions. Part I Timoshenko–Mindlin shell theory

G.M. Kulikov *, S.V. Plotnikova

Department of Applied Mathematics and Mechanics, Tambov State Technical University, Sovetskaya Street, 106 Tambov 392000, Russia

Received 22 March 2002; received in revised form 14 October 2002

Abstract

The precise representation of arbitrarily large rigid-body motions in the displacement patterns of curved Timoshenko–Mindlin (TM) shell elements is considered. This consideration requires the development of the strain–displacement relationships of the finite deformation TM shell theory with regard to their consistency with the large rigid-body motions. For this purpose a refined TM theory of multilayered anisotropic shells undergoing finite deformations is elaborated. The transverse shear and transverse normal deformation response and bending–extension coupling are included. The fundamental unknowns consist of six displacements and 11 strains of the bottom and top surfaces of the shell, and 11 stress resultants. On the basis of this theory the simple and efficient mixed models are developed by using the incremental total Lagrangian formulation in conjunction with the Newton–Raphson method. The elemental arrays are derived applying the Hu–Washizu mixed variational principle. Numerical results are presented to demonstrate the high accuracy and effectiveness of the developed four-node shell elements and to compare their performance with other non-linear finite elements reported in the literature.

Keywords: Timoshenko–Mindlin element; Mixed model; Large rigid-body motion; Multilayered shell

1. Introduction

Using the traditional non-linear Timoshenko–Mindlin (TM) theory in a finite-element (FE) formulation for plates and shells is well established and has been shown to give acceptable results [1–15]. This theory has the advantage that displacement and rotation trial functions may be used and these functions need only to be C^0 continuous. The developed refined non-linear TM shell theory has the essential advantage, since herein as unknown functions six displacements of the face surfaces of the shell are chosen [16–18]. In a result, only independent trial functions of displacements of the face surfaces may be used. This allows

* Corresponding author. Fax: +7-075-253-2017.
E-mail address: kulikov@apmath.tstu.ru (G.M. Kulikov).
URL: http://apm.tstu.ru/kulikov.

0045-7825/03/$ - see front matter © 2002 Published by Elsevier Science B.V.
PII: S0045-7825(02)00601-1

special loading conditions at the face surfaces of the shell to be accounted for. Besides, such choice of displacements gives the possibility to deduce the non-linear strain–displacement equations, which are completely free for all large rigid-body motions.

One of the main requirements of the modern shell theory that is intended for the general non-linear FE formulation is that it must lead to strain-free modes for arbitrarily large rigid-body motions. The adequate representation of large rigid-body motions is a necessary condition if a non-linear element is to have the good accuracy and convergence properties. Therefore, when an inconsistent non-linear shell theory is used to construct any finite element, erroneous straining modes under arbitrarily large rigid-body motions may be appeared. This problem has been studied for the geometrically linear TM shell theory in Refs. [19,20] and for the finite deformation Timoshenko beam theory in Ref. [21]. Herein, the more general study on the basis of the refined finite deformation TM shell theory taking into account the transverse normal deformation response and bending–extension coupling is considered.

It is well known that in some works (see Refs. [22–25], among others) developing the solid shell concept displacement vectors of the bottom and top surfaces are also used and resolved with respect to some global Cartesian basis in order to exactly describe rigid-body motions. But in our TM shell theory selecting as unknowns the displacements of the bottom and top surfaces has a principally another mechanical sense and allows one to formulate any curved TM shell element with very attractive properties, since *only* in this case we can deduce non-linear strain–displacement relationships that are objective, i.e., invariant under rigid-body motions. Taking into account that herein the displacement vectors of the face surfaces are represented in the local reference surface basis, the developed FE formulation has substantial computational advantages compared to the conventional isoparametric FE formulations, since it eliminates the costly numerical integration by deriving the stiffness matrices. Indeed, our element matrix requires only direct substitutions (no inversion is needed if an element is rectangular) and it is evaluated by using the full exact analytical integration.

The proposed theory is free of assumptions of small displacements, small rotations and small loading steps because herein the *exact* shell theory based on the objective fully non-linear strain–displacement relationships is discussed. There exists only one limitation associated with a simple fact that the loading step cannot be too large. This restriction arises in the case of using the Newton–Raphson method, since the iteration process can be diverged due to an escape of the initial trial value from Newton's attractive area. An important feature of the developed formulation is that no enhanced strains [4–6,12,26–28] are needed to obtain the computationally exact solutions of the bending dominated shell problems and no Poisson thickness locking [24,27,28] can occur when Poisson's ratios are not zero.

The FE formulation is based on a simple and efficient approximation of plates and shells via quadrilateral four-node elements developed by Hughes and Tezduyar [29], and by Wempner et al. [30]. The fundamental unknowns consist of six displacements and 11 strains of the face surfaces of the shell, and 11 stress resultants. The simplest admissible approximations of the two-dimensional fields are used, namely, bilinear approximations of the displacements, and assumed approximations of the strains and stress resultants. The elemental arrays are obtained by using the Hu–Washizu mixed variational principle in conjunction with the incremental total Lagrangian formulation and Newton–Raphson method.

The numerical results are presented to demonstrate the efficiency and high accuracy of the developed finite deformation TM shell theory and to compare it with other theories reported in the literature. For this purpose five tests are employed.

2. Strain–displacement equations

Let us consider a shell of uniform thickness h. The shell may be defined as a 3-D body of volume V bounded by two bounding surfaces S^- and S^+, located at the distances δ^- and δ^+ measured with respect to

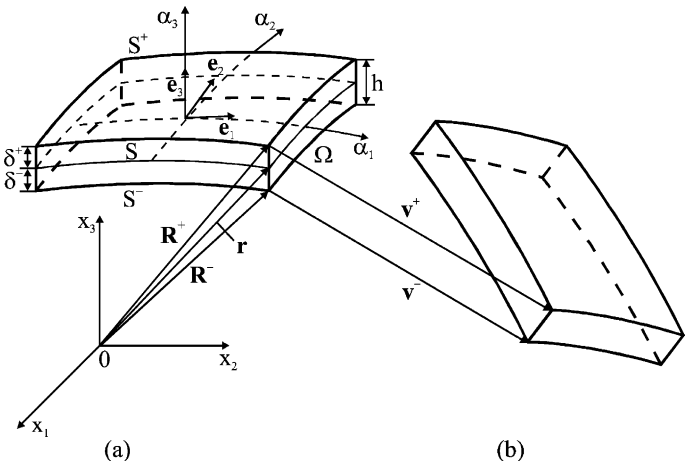

Fig. 1. Geometry and kinematics of the shell: (a) initial configuration and (b) current configuration.

the reference surface S, and the edge boundary surface Ω that is perpendicular to the reference surface (see Fig. 1). Let the reference surface S be referred to an orthogonal curvilinear coordinate system α_1 and α_2, which coincides with the lines of principal curvatures of its surface; $\mathbf{e}_1$ and $\mathbf{e}_2$ denote the tangent unit vectors to the lines of principal curvatures. The α_3-axis is oriented along the unit vector $\mathbf{e}_3$ normal to the reference surface. The initial configuration of the shell at time t_0 is shown in Fig. 1(a) while Fig. 1(b) illustrates the current configuration at time t.

The curvilinear components of the Green–Lagrange strain tensor for the finite deformation analysis [31] can be written in a vector form as

$$2\varepsilon^{e}_{ij} = \frac{1}{H_i}\mathbf{u}_{,i}\left(\mathbf{e}_j + \frac{1}{2H_j}\mathbf{u}_{,j}\right) + \frac{1}{H_j}\mathbf{u}_{,j}\left(\mathbf{e}_i + \frac{1}{2H_i}\mathbf{u}_{,i}\right), \tag{1a}$$

$$\mathbf{u} = \sum_i u_i \mathbf{e}_i, \tag{1b}$$

$$H_\alpha = A_\alpha(1 + k_\alpha\alpha_3), \quad H_3 = 1, \tag{1c}$$

where $u_i(\alpha_1, \alpha_2, \alpha_3)$ are the components of the displacement vector, which are always measured in accordance with the total Lagrangian formulation from the initial configuration to the current configuration directly (see Fig. 1); A_α and k_α are the Lamé coefficients and principal curvatures of the reference surface; H_α are the Lamé coefficients of any surface parallel to the reference surface. Here and in the following developments the abbreviation $(\ )_{,i}$ implies the partial derivative with respect to the coordinate α_i, and indices i, j, ℓ, m take the values 1, 2 and 3 while Greek indices α, β, γ, δ take the values 1 and 2.

The refined finite deformation TM shell theory is based on the linear approximation of the displacements in the thickness direction [16,17]:

$$\mathbf{u} = N^-(\alpha_3)\mathbf{v}^- + N^+(\alpha_3)\mathbf{v}^+, \tag{2a}$$

$$\mathbf{v}^\pm = \sum_i v_i^\pm \mathbf{e}_i, \tag{2b}$$

$$N^-(\alpha_3) = (\delta^+ - \alpha_3)/h, \qquad N^+(\alpha_3) = (\alpha_3 - \delta^-)/h, \tag{2c}$$

where $v_i^{\pm}(\alpha_1,\alpha_2)$ are the displacements of the face surfaces $S^{\pm}$; $N^{\pm}(\alpha_3)$ are the linear shape functions. The linear approximation (2) may be treated as a refined Timoshenko kinematic hypothesis [32,33]. The advantage of the proposed approach is apparent because the special loading conditions at the face surfaces and shell edges can be formulated. Moreover, this simplifies a formulation of new FE models [19–21] and provides a convenient way to express the non-linear strain–displacement relationships in terms of face surface strains as we shall see below.

Substituting displacements (2a) into the strain–displacement equations (1a) and taking into account formulas for the derivatives of the unit vector $\mathbf{e}_3$ with respect to the coordinates α_1 and α_2 [34]

$$\mathbf{e}_{3,\alpha} = A_\alpha k_\alpha \mathbf{e}_\alpha,$$

one can obtain the strain–displacement equations of the finite deformation TM theory of *thick* shells:

$$\begin{aligned} 2\varepsilon^a_{\alpha\beta} = {} & \left[N^-(\alpha_3)\frac{1}{H_\alpha}\mathbf{v}^-_{,\alpha} + N^+(\alpha_3)\frac{1}{H_\alpha}\mathbf{v}^+_{,\alpha}\right]\mathbf{e}_\beta + \left[N^-(\alpha_3)\frac{1}{H_\beta}\mathbf{v}^-_{,\beta} + N^+(\alpha_3)\frac{1}{H_\beta}\mathbf{v}^+_{,\beta}\right]\mathbf{e}_\alpha \\ & + \left[N^-(\alpha_3)\frac{1}{H_\alpha}\mathbf{v}^-_{,\alpha} + N^+(\alpha_3)\frac{1}{H_\alpha}\mathbf{v}^+_{,\alpha}\right]\left[N^-(\alpha_3)\frac{1}{H_\beta}\mathbf{v}^-_{,\beta} + N^+(\alpha_3)\frac{1}{H_\beta}\mathbf{v}^+_{,\beta}\right], \end{aligned} \tag{3a}$$

$$2\varepsilon^a_{\alpha 3} = \frac{\overline{H}_\alpha}{H_\alpha}\boldsymbol{\beta}\mathbf{e}_\alpha + \frac{1}{H_\alpha}\bar{\mathbf{v}}_{,\alpha}(\mathbf{e}_3+\boldsymbol{\beta}) + (\alpha_3-\bar{\delta})\frac{1}{H_\alpha}\varepsilon^a_{33,\alpha}, \tag{3b}$$

$$\varepsilon^a_{33} = \boldsymbol{\beta}\left(\mathbf{e}_3+\frac{1}{2}\boldsymbol{\beta}\right), \quad \boldsymbol{\beta} = \frac{1}{h}(\mathbf{v}^+-\mathbf{v}^-), \quad \bar{\mathbf{v}} = \tfrac{1}{2}(\mathbf{v}^-+\mathbf{v}^+), \tag{3c}$$

where $\bar{\delta} = (\delta^- + \delta^+)/2$ is the distance from the reference surface to the middle surface; $\overline{H}_\alpha = A_\alpha(1+k_\alpha\bar{\delta})$ are the Lamé coefficients of the middle surface.

Replacing further Lamé coefficients H_α by their values on the top and bottom surfaces $H^{\pm}_\alpha = A_\alpha(1+k_\alpha\delta^{\pm})$ in formulas (3a) for the tangential strains and by their values on the middle surface $\overline{H}_\alpha$ in formulas (3b) for the transverse shear strains, the strain–displacement equations of the finite deformation TM theory of the *moderately thick* shells are obtained

$$\begin{aligned} 2\varepsilon^b_{\alpha\beta} = {} & \left[N^-(\alpha_3)\frac{1}{H^-_\alpha}\mathbf{v}^-_{,\alpha} + N^+(\alpha_3)\frac{1}{H^+_\alpha}\mathbf{v}^+_{,\alpha}\right]\mathbf{e}_\beta + \left[N^-(\alpha_3)\frac{1}{H^-_\beta}\mathbf{v}^-_{,\beta} + N^+(\alpha_3)\frac{1}{H^+_\beta}\mathbf{v}^+_{,\beta}\right]\mathbf{e}_\alpha \\ & + \left[N^-(\alpha_3)\frac{1}{H^-_\alpha}\mathbf{v}^-_{,\alpha} + N^+(\alpha_3)\frac{1}{H^+_\alpha}\mathbf{v}^+_{,\alpha}\right]\left[N^-(\alpha_3)\frac{1}{H^-_\beta}\mathbf{v}^-_{,\beta} + N^+(\alpha_3)\frac{1}{H^+_\beta}\mathbf{v}^+_{,\beta}\right], \end{aligned} \tag{4a}$$

$$2\varepsilon^b_{\alpha 3} = \boldsymbol{\beta}\mathbf{e}_\alpha + \frac{1}{\overline{H}_\alpha}\bar{\mathbf{v}}_{,\alpha}(\mathbf{e}_3+\boldsymbol{\beta}) + (\alpha_3-\bar{\delta})\frac{1}{\overline{H}_\alpha}\varepsilon^b_{33,\alpha}, \tag{4b}$$

$$\varepsilon^b_{33} = \boldsymbol{\beta}\left(\mathbf{e}_3+\frac{1}{2}\boldsymbol{\beta}\right), \quad \boldsymbol{\beta} = \frac{1}{h}(\mathbf{v}^+-\mathbf{v}^-), \quad \bar{\mathbf{v}} = \tfrac{1}{2}(\mathbf{v}^-+\mathbf{v}^+). \tag{4c}$$

The strain–displacement equations (4) are more attractive than (3) because they are completely free for arbitrarily large rigid-body motions. It will be shown in the next section. Note also that tangential strains $\varepsilon^b_{\alpha\beta}$ are distributed over the shell thickness according to the quadratic law. Taking into account that a shell has a moderate thickness, this complication of the TM shell theory would be unreasonable because of the minor significance of the quadratic terms in most problems.

Therefore, more convenient strain–displacement equations of the finite deformation TM theory of the *moderately thick* shells can be written as

$$2\varepsilon^c_{\alpha\beta} = N^-(\alpha_3)\left(\frac{1}{H^-_\alpha}\mathbf{v}^-_{,\alpha}\mathbf{e}_\beta + \frac{1}{H^-_\beta}\mathbf{v}^-_{,\beta}\mathbf{e}_\alpha + \frac{1}{H^-_\alpha H^-_\beta}\mathbf{v}^-_{,\alpha}\mathbf{v}^-_{,\beta}\right) + N^+(\alpha_3)\left(\frac{1}{H^+_\alpha}\mathbf{v}^+_{,\alpha}\mathbf{e}_\beta + \frac{1}{H^+_\beta}\mathbf{v}^+_{,\beta}\mathbf{e}_\alpha + \frac{1}{H^+_\alpha H^+_\beta}\mathbf{v}^+_{,\alpha}\mathbf{v}^+_{,\beta}\right), \tag{5a}$$

$$2\varepsilon^c_{\alpha 3} = \boldsymbol{\beta}\mathbf{e}_\alpha + \frac{1}{\overline{H}_\alpha}\bar{\mathbf{v}}_{,\alpha}(\mathbf{e}_3 + \boldsymbol{\beta}) + (\alpha_3 - \bar{\delta})\frac{1}{\overline{H}_\alpha}\varepsilon^c_{33,\alpha}, \tag{5b}$$

$$\varepsilon^c_{33} = \boldsymbol{\beta}\left(\mathbf{e}_3 + \frac{1}{2}\boldsymbol{\beta}\right), \quad \boldsymbol{\beta} = \frac{1}{h}(\mathbf{v}^+ - \mathbf{v}^-), \quad \bar{\mathbf{v}} = \tfrac{1}{2}(\mathbf{v}^- + \mathbf{v}^+). \tag{5c}$$

These strain–displacement equations are also completely free for large rigid-body motions. It will be discussed in Section 3.

It is important to note that strain–displacement equations (3)–(5) satisfy the following coupling conditions:

$$\begin{aligned}
&\varepsilon^a_{\alpha\alpha}(\delta^\pm) = \varepsilon^b_{\alpha\alpha}(\delta^\pm) = \varepsilon^c_{\alpha\alpha}(\delta^\pm) = E^\pm_{\alpha\alpha},\\
&2\varepsilon^a_{12}(\delta^\pm) = 2\varepsilon^b_{12}(\delta^\pm) = 2\varepsilon^c_{12}(\delta^\pm) = E^\pm_{12},\\
&2\varepsilon^a_{\alpha 3}(\bar{\delta}) = 2\varepsilon^b_{\alpha 3}(\bar{\delta}) = 2\varepsilon^c_{\alpha 3}(\bar{\delta}) = \overline{E}_{\alpha 3},
\end{aligned} \tag{6}$$

where $E^\pm_{\alpha\beta}$ are the tangential strains of the face surfaces $S^\pm$; $\overline{E}_{\alpha 3}$ are the transverse shear strains of the middle surface, which are defined as

$$\begin{aligned}
E^\pm_{\alpha\alpha} &= \frac{1}{H^\pm_\alpha}\mathbf{v}^\pm_{,\alpha}\mathbf{e}_\alpha + \frac{1}{2}\left(\frac{1}{H^\pm_\alpha}\mathbf{v}^\pm_{,\alpha}\right)^2,\\
E^\pm_{12} &= \frac{1}{H^\pm_1}\mathbf{v}^\pm_{,1}\mathbf{e}_2 + \frac{1}{H^\pm_2}\mathbf{v}^\pm_{,2}\mathbf{e}_1 + \frac{1}{H^\pm_1 H^\pm_2}\mathbf{v}^\pm_{,1}\mathbf{v}^\pm_{,2},\\
\overline{E}_{\alpha 3} &= \boldsymbol{\beta}\mathbf{e}_\alpha + \frac{1}{\overline{H}_\alpha}\bar{\mathbf{v}}_{,\alpha}(\mathbf{e}_3 + \boldsymbol{\beta}).
\end{aligned} \tag{7}$$

This statement is illustrated in Fig. 2.

More simple strain–displacement equations can be obtained for the *thin* shells replacing the Lamé coefficients H_α by the Lamé coefficients of the middle surface $\overline{H}_\alpha$ in formulas (3a) and (3b), and neglecting again the quadratic non-linear terms. As a result we have

$$2\varepsilon^d_{\alpha\beta} = N^-(\alpha_3)\left(\frac{1}{\overline{H}_\alpha}\mathbf{v}^-_{,\alpha}\mathbf{e}_\beta + \frac{1}{\overline{H}_\beta}\mathbf{v}^-_{,\beta}\mathbf{e}_\alpha + \frac{1}{\overline{H}_\alpha\overline{H}_\beta}\mathbf{v}^-_{,\alpha}\mathbf{v}^-_{,\beta}\right) + N^+(\alpha_3)\left(\frac{1}{\overline{H}_\alpha}\mathbf{v}^+_{,\alpha}\mathbf{e}_\beta + \frac{1}{\overline{H}_\beta}\mathbf{v}^+_{,\beta}\mathbf{e}_\alpha + \frac{1}{\overline{H}_\alpha\overline{H}_\beta}\mathbf{v}^+_{,\alpha}\mathbf{v}^+_{,\beta}\right), \tag{8a}$$

$$2\varepsilon^d_{\alpha 3} = \boldsymbol{\beta}\mathbf{e}_\alpha + \frac{1}{\overline{H}_\alpha}\bar{\mathbf{v}}_{,\alpha}(\mathbf{e}_3 + \boldsymbol{\beta}) + (\alpha_3 - \bar{\delta})\frac{1}{\overline{H}_\alpha}\varepsilon^d_{33,\alpha}, \tag{8b}$$

$$\varepsilon^d_{33} = \boldsymbol{\beta}\left(\mathbf{e}_3 + \frac{1}{2}\boldsymbol{\beta}\right), \quad \boldsymbol{\beta} = \frac{1}{h}(\mathbf{v}^+ - \mathbf{v}^-), \quad \bar{\mathbf{v}} = \tfrac{1}{2}(\mathbf{v}^- + \mathbf{v}^+). \tag{8c}$$

As we shall see in the next section, the strain–displacement equations (8) can never be free for large rigid-body motions.

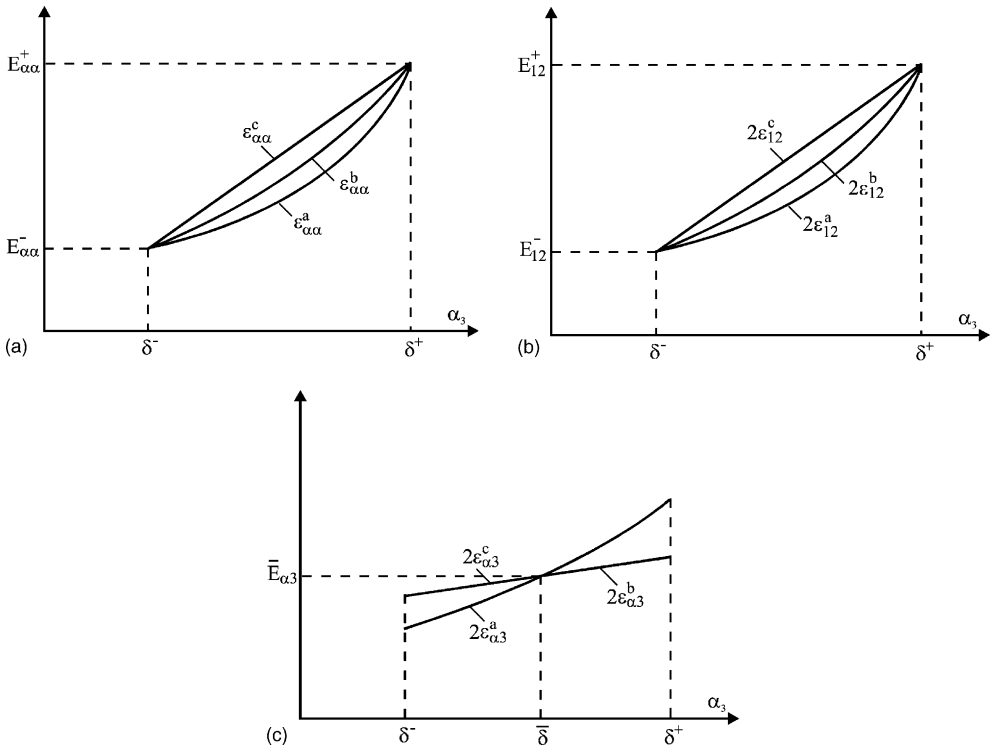

Fig. 2. Distribution of strains over the shell thickness.

3. Large rigid-body motions

An arbitrarily large rigid-body motion can be defined as

$$\mathbf{u}^{\mathrm{Rigid}} = \mathbf{\Delta} + (\mathbf{A} - \mathbf{E})\mathbf{R}, \tag{9}$$

where $\mathbf{R} = \mathbf{r} + \alpha_3\mathbf{e}_3$ is the position vector of any point of the shell; $\mathbf{r}$ is the position vector of any point of the reference surface; $\mathbf{\Delta} = \sum_i \Delta_i \mathbf{e}_i$ is the constant displacement (translation) vector; $\mathbf{E}$ is the identity matrix; $\mathbf{A}$ is the orthogonal rotation matrix.

In particular, rigid-body motions of the face surfaces are

$$\mathbf{v}^{\pm\mathrm{Rigid}} = \mathbf{\Delta} + (\mathbf{A} - \mathbf{E})\mathbf{R}^{\pm}, \tag{10}$$

where $\mathbf{R}^{\pm} = \mathbf{r} + \delta^{\pm}\mathbf{e}_3$ are the position vectors of points of the face surfaces $S^{\pm}$.

The derivatives of the translation and position vectors can be written as

$$\mathbf{\Delta}_{,\alpha} = \mathbf{0}, \quad \mathbf{r}_{,\alpha} = A_\alpha \mathbf{e}_\alpha. \tag{11}$$

Taking into account formulas (10) and (11), and expressions for the derivatives of the normal unit vector of the reference surface with respect to the coordinates α_1 and α_2 (see Section 2), one obtains

$$\mathbf{v}^{\pm\mathrm{Rigid}}_{,\alpha} = H^{\pm}_{\alpha}(\mathbf{A}\mathbf{e}_\alpha - \mathbf{e}_\alpha). \tag{12}$$

It can be verified by using Eqs. (10) and (12) that modified strains from relationships (4) are all zero in a general large rigid-body motion, i.e.,

$$2\varepsilon_{\alpha\beta}^{b\text{Rigid}} = (\mathbf{A}\mathbf{e}_\alpha)(\mathbf{A}\mathbf{e}_\beta) - \mathbf{e}_\alpha\mathbf{e}_\beta = 0, \quad 2\varepsilon_{33}^{b\text{Rigid}} = (\mathbf{A}\mathbf{e}_3)(\mathbf{A}\mathbf{e}_3) - \mathbf{e}_3\mathbf{e}_3 = 0,$$
$$2\varepsilon_{\alpha 3}^{b\text{Rigid}} = \frac{H_\alpha}{\overline{H}_\alpha}[(\mathbf{A}\mathbf{e}_\alpha)(\mathbf{A}\mathbf{e}_3) - \mathbf{e}_\alpha\mathbf{e}_3] = 0. \tag{13}$$

This conclusion is true because an orthogonal transformation retains the scalar product of the vectors.

Using again Eqs. (10) and (12) into the strain–displacement relationships (5), and allowing for a property of the orthogonal transformation **A**, one can get the following result:

$$2\varepsilon_{ij}^{c\text{Rigid}} = 0. \tag{14}$$

A proof of the more general proposition is given in Appendix A.

So, our finite deformation TM shell theories based on the modified strain–displacement relationships (4) and (5) are completely strain-free for all large rigid-body motions. It should be noted that using a similar technique the more general finite deformation layer-wise TM shell theory [35] could be developed. This theory is under development and will be published in the next paper.

Finally, one can verify that the finite deformation TM shell theory based on relationships (8) can never be strain-free for large rigid-body motions, since $\varepsilon_{\alpha\beta}^{d\text{Rigid}} \neq 0$ for shells of arbitrary geometry. Note that it is a serious deficiency of this finite deformation TM shell theory.

4. Hu–Washizu functional for multilayered anisotropic shell

Let us consider a shell built up in the general case by the arbitrary superposition across the wall thickness of N layers of uniform thickness h_k. The kth layer may be defined as a 3-D body of volume V_k bounded by two surfaces S_{k-1} and S_k, located at the distances δ_{k-1} and δ_k measured with respect to the reference surface S, and the edge boundary surface Ω_k (see Fig. 3). The full edge boundary surface $\Omega = \Omega_1 + \Omega_2 + \cdots + \Omega_N$ is generated by the normals to the reference surface along the bounding curve Γ (with the arc length s) of this surface. It is also assumed that the bounding surfaces S_{k-1} and S_k are continuous, sufficiently smooth and without any singularities. Let the reference surface S be referred to an orthogonal curvilinear coordinate

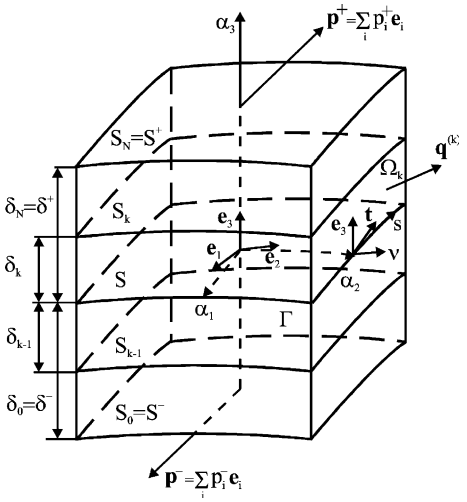

Fig. 3. Geometry of the multilayered shell.

system α_1 and α_2, which coincides with the lines of principal curvatures of its surface. The α_3-axis is oriented along the normal direction.

The constituent layers of the shell are supposed to be rigidly joined, so that no slip on contact surfaces and no separation of layers can occur. The material of each constituent layer is assumed to be linearly elastic, anisotropic, homogeneous or fiber reinforced, such that in each point there is a single surface of elastic symmetry parallel to the reference surface. Let p_i^- and p_i^+ be the intensities of the external loading acting on the bottom surface $S^- = S_0$ and top surface $S^+ = S_N$ in the α_i coordinate directions, respectively, while $\mathbf{q}^{(k)} = q_\nu^{(k)}\boldsymbol{\nu} + q_t^{(k)}\mathbf{t} + q_3^{(k)}\mathbf{e}_3$ be the external loading vector acting on the edge boundary surface Ω_k, where $q_\nu^{(k)}$, $q_t^{(k)}$ and $q_3^{(k)}$ are the components of its vector in the ν, t and α_3 directions; $\boldsymbol{\nu}$ and $\mathbf{t}$ are the normal and tangential unit vectors to the bounding curve Γ (see Fig. 3). Here and in the following developments the index $k = \overline{1,N}$ identifies the belonging of any quantity to the kth layer.

The finite deformation TM theory of multilayered anisotropic shells is based on the linear approximation of the displacement vector in the thickness direction (2), where we should set $\delta^- = \delta_0$ and $\delta^+ = \delta_N$. Substituting displacements (2) and strains rewritten in the more convenient form (see Fig. 2)

$$\begin{aligned} &\varepsilon_{\alpha\alpha} = N^-(\alpha_3)E_{\alpha\alpha}^- + N^+(\alpha_3)E_{\alpha\alpha}^+, \quad \varepsilon_{33} = E_{33}, \\ &2\varepsilon_{ij} = N^-(\alpha_3)E_{ij}^- + N^+(\alpha_3)E_{ij}^+ \quad (i \neq j) \end{aligned} \tag{15}$$

into the Hu–Washizu functional [31], and allowing for the objective strain–displacement relationships (5), one can obtain

$$\begin{aligned} J = \iint_S \Bigg\{ & \Pi - \sum_{\alpha \leqslant i} \left[\mathscr{H}_{\alpha i}^-(E_{\alpha i}^- - e_{\alpha i}^- - \eta_{\alpha i}^-) + \mathscr{H}_{\alpha i}^+(E_{\alpha i}^+ - e_{\alpha i}^+ - \eta_{\alpha i}^+) \right] \\ & - \mathscr{H}_{33}(E_{33} - e_{33} - \eta_{33}) + \sum_i \left(p_i^- v_i^- - p_i^+ v_i^+ \right) \Bigg\} A_1 A_2 \bar{\zeta}_1 \bar{\zeta}_2 \, \mathrm{d}\alpha_1 \, \mathrm{d}\alpha_2 \\ & - \oint_\Gamma \left(\hat{\mathscr{H}}_{\nu\nu}^- v_\nu^- + \hat{\mathscr{H}}_{\nu\nu}^+ v_\nu^+ + \hat{\mathscr{H}}_{\nu t}^- v_t^- + \hat{\mathscr{H}}_{\nu t}^+ v_t^+ + \hat{\mathscr{H}}_{\nu 3}^- v_3^- + \hat{\mathscr{H}}_{\nu 3}^+ v_3^+ \right) \bar{\gamma} \, \mathrm{d}s, \end{aligned} \tag{16}$$

where

$$e_{\alpha\alpha}^\pm = \frac{1}{\zeta_\alpha^\pm}\lambda_\alpha^\pm, \quad e_{12}^\pm = \frac{1}{\zeta_1^\pm}\omega_1^\pm + \frac{1}{\zeta_2^\pm}\omega_2^\pm, \quad e_{\alpha 3}^\pm = \left(1 \pm \frac{k_\alpha h}{2\bar{\zeta}_\alpha}\right)\beta_\alpha - \frac{1}{\bar{\zeta}_\alpha}\theta_\alpha^\pm, \quad e_{33} = \beta_3, \tag{17}$$

$$\eta_{\alpha\alpha}^\pm = \frac{1}{2(\zeta_\alpha^\pm)^2}\left[(\lambda_\alpha^\pm)^2 + (\omega_\alpha^\pm)^2 + (\theta_\alpha^\pm)^2\right], \quad \eta_{12}^\pm = \frac{1}{\zeta_1^\pm \zeta_2^\pm}(\lambda_1^\pm\omega_2^\pm + \lambda_2^\pm\omega_1^\pm + \theta_1^\pm\theta_2^\pm),$$

$$\eta_{\alpha 3}^\pm = \frac{1}{\bar{\zeta}_\alpha}(\beta_\alpha\lambda_\alpha^\pm + \beta_\delta\omega_\alpha^\pm - \beta_3\theta_\alpha^\pm), \quad \eta_{33} = \tfrac{1}{2}(\beta_1^2 + \beta_2^2 + \beta_3^2),$$

$$\lambda_\alpha^\pm = \frac{1}{A_\alpha}v_{\alpha,\alpha}^\pm + B_\delta v_\delta^\pm + k_\alpha v_3^\pm, \quad \omega_\alpha^\pm = \frac{1}{A_\alpha}v_{\delta,\alpha}^\pm - B_\delta v_\alpha^\pm,$$

$$\theta_\alpha^\pm = -\frac{1}{A_\alpha}v_{3,\alpha}^\pm + k_\alpha v_\alpha^\pm, \quad \beta_i = \frac{1}{h}(v_i^+ - v_i^-), \quad \bar{\gamma} = 1 + k_N\bar{\delta},$$

$$\zeta_\alpha^\pm = 1 + k_\alpha\delta^\pm, \quad \bar{\zeta}_\alpha = 1 + k_\alpha\bar{\delta}, \quad B_\alpha = \frac{1}{A_1A_2}A_{\delta,\alpha} \quad (\delta \neq \alpha).$$

Here, $\Pi(E^{\pm}_{\alpha i}, E_{33})$ is the strain energy density; $v^{\pm}_{\nu}$, $v^{\pm}_{t}$ and $v^{\pm}_{3}$ are the components of the displacement vectors of the face surfaces in the coordinate system ν, t and α_3 (see Fig. 3); k_N is the normal curvature of the bounding curve Γ; $\mathscr{H}^{\pm}_{\alpha i}$ and $\mathscr{H}_{33}$ are the stress resultants; $\hat{\mathscr{H}}^{\pm}_{\nu\nu}$, $\hat{\mathscr{H}}^{\pm}_{\nu t}$ and $\hat{\mathscr{H}}^{\pm}_{\nu 3}$ are the external load resultants, which are defined as

$$\Pi = \frac{1}{2}\sum_{i\leqslant j}\sum_{\ell\leqslant m}\left[D^{00}_{ij\ell m}E^{-}_{ij}E^{-}_{\ell m} + D^{01}_{ij\ell m}\left(E^{-}_{ij}E^{+}_{\ell m} + E^{+}_{ij}E^{-}_{\ell m}\right) + D^{11}_{ij\ell m}E^{+}_{ij}E^{+}_{\ell m}\right], \tag{18}$$

$$D^{pq}_{ij\ell m} = \sum_{k}\int_{\delta_{k-1}}^{\delta_k} C^{(k)}_{ij\ell m}[N^{-}(\alpha_3)]^{2-p-q}[N^{+}(\alpha_3)]^{p+q}\,\mathrm{d}\alpha_3 \quad (p,q=0,1), \tag{19}$$

$$\mathscr{H}^{\pm}_{\alpha i} = \sum_{k}\int_{\delta_{k-1}}^{\delta_k} S^{(k)}_{\alpha i}N^{\pm}(\alpha_3)\,\mathrm{d}\alpha_3, \qquad \mathscr{H}_{33} = \sum_{k}\int_{\delta_{k-1}}^{\delta_k} S^{(k)}_{33}\,\mathrm{d}\alpha_3, \tag{20}$$

$$\hat{\mathscr{H}}^{\pm}_{\nu r} = \sum_{k}\int_{\delta_{k-1}}^{\delta_k} q^{(k)}_{r}N^{\pm}(\alpha_3)\,\mathrm{d}\alpha_3 \quad (r=\nu,t,3),$$

where $S^{(k)}_{ij}$ are the components of the second Piola–Kirchhoff stress tensor of the kth layer; $C^{(k)}_{ij\ell m}$ are the components of the elasticity tensor of the kth layer. Besides, we should set into Eqs. (18) and (19) $E^{-}_{33} = E^{+}_{33} = E_{33}$ and $C^{(k)}_{\alpha\beta\gamma 3} = C^{(k)}_{\alpha 333} = 0$, correspondingly.

5. Stress–strain equations

Stresses in formulas (20) can be found by using the complete 3-D stress–strain relationships as

$$S^{(k)}_{ij} = \sum_{\ell,m} C^{(k)}_{ij\ell m}\varepsilon_{\ell m}. \tag{21}$$

In the case of the multilayered isotropic shell we have the following expressions for the material moduli:

$$\begin{aligned} &C^{(k)}_{1111} = C^{(k)}_{2222} = C^{(k)}_{3333} = (1-\nu_k)\lambda_k/\nu_k, \qquad C^{(k)}_{1122} = C^{(k)}_{1133} = C^{(k)}_{2233} = \lambda_k,\\ &C^{(k)}_{1212} = C^{(k)}_{1313} = C^{(k)}_{2323} = \frac{E_k}{2(1+\nu_k)}, \qquad \lambda_k = \frac{\nu_k E_k}{(1+\nu_k)(1-2\nu_k)},\\ &C^{(k)}_{1112} = C^{(k)}_{2212} = C^{(k)}_{3312} = C^{(k)}_{1323} = 0, \end{aligned} \tag{22}$$

where E_k and ν_k are Young's modulus and Poisson's ratio of the kth layer.

Unfortunately, such a formulation on the basis of the complete 3-D constitutive law is deficient because so-called Poisson thickness locking [27,28] can occur. This phenomenon occurs in bending dominated shell problems when Poisson's ratios of layers are not equal to zero. The main reason is that the Poisson effect in the thickness direction is taken into account in equations of Hooke's law for the tangential strains.

To avoid Poisson thickness locking, we should simplify the first three equations of the constitutive law (21) omitting the thickness strain:

$$S^{(k)}_{\alpha\beta} = \sum_{\gamma,\delta} C^{(k)}_{\alpha\beta\gamma\delta}\varepsilon_{\gamma\delta}, \tag{23a}$$

i.e., $C^{(k)}_{\alpha\beta 33}=0$. It is apparent that this simplification needs to be done and in Eqs. (18) and (19) for the strain energy density (see for details Ref. [20]). The remaining equations are taken without changes:

$$S^{(k)}_{33}=\sum_{\gamma,\delta}C^{(k)}_{33\gamma\delta}\varepsilon_{\gamma\delta}+C^{(k)}_{3333}\varepsilon_{33}, \tag{23b}$$

$$S^{(k)}_{\alpha 3}=2\sum_{\gamma}C^{(k)}_{\alpha 3\gamma 3}\varepsilon_{\gamma 3}. \tag{23c}$$

In order to substantiate our simplification, we consider an orthotropic layer of the shell whose axes of symmetry $\alpha^{(k)}_{1'}$ and $\alpha^{(k)}_{2'}$ do not coincide with the coordinate directions α_1 and α_2. In axes of symmetry the equations of the complete 3-D Hooke's law will be

$$\varepsilon_{1'1'}=\frac{1}{E^{(k)}_1}S^{(k)}_{1'1'}-\frac{v^{(k)}_{21}}{E^{(k)}_2}S^{(k)}_{2'2'}-\frac{v^{(k)}_{31}}{E^{(k)}_3}S^{(k)}_{33},\qquad \varepsilon_{2'2'}=-\frac{v^{(k)}_{12}}{E^{(k)}_1}S^{(k)}_{1'1'}+\frac{1}{E^{(k)}_2}S^{(k)}_{2'2'}-\frac{v^{(k)}_{32}}{E^{(k)}_3}S^{(k)}_{33}, \tag{24a}$$

$$\varepsilon_{33}=-\frac{v^{(k)}_{13}}{E^{(k)}_1}S^{(k)}_{1'1'}-\frac{v^{(k)}_{23}}{E^{(k)}_2}S^{(k)}_{2'2'}+\frac{1}{E^{(k)}_3}S^{(k)}_{33}, \tag{24b}$$

$$2\varepsilon_{1'2'}=\frac{1}{G^{(k)}_{12}}S^{(k)}_{1'2'},\quad 2\varepsilon_{1'3}=\frac{1}{G^{(k)}_{13}}S^{(k)}_{1'3},\quad 2\varepsilon_{2'3}=\frac{1}{G^{(k)}_{23}}S^{(k)}_{2'3}, \tag{24c}$$

where $E^{(k)}_1$, $E^{(k)}_2$ and $E^{(k)}_3$ are the elastic moduli in the $\alpha^{(k)}_{1'}$, $\alpha^{(k)}_{2'}$ and α_3 directions; $G^{(k)}_{12}$, $G^{(k)}_{13}$ and $G^{(k)}_{23}$ are the shear moduli; $v^{(k)}_{ij}$ are Poisson's ratios. From reasons of symmetry, we have

$$\frac{v^{(k)}_{ij}}{E^{(k)}_i}=\frac{v^{(k)}_{ji}}{E^{(k)}_j}\quad \text{for } i\neq j.$$

With exactitude acceptable to shell structures it is possible to adopt the following assumption:

$$S^{(k)}_{33}\ll S^{(k)}_{1'1'},S^{(k)}_{2'2'}. \tag{25}$$

Then, neglecting in accordance with formula (25) the transverse normal stress in Eq. (24a) and solving for the tangential normal stresses, one can find

$$\begin{aligned}&S^{(k)}_{1'1'}=Q^{(k)}_{11}\varepsilon_{1'1'}+Q^{(k)}_{12}\varepsilon_{2'2'},\quad S^{(k)}_{2'2'}=Q^{(k)}_{12}\varepsilon_{1'1'}+Q^{(k)}_{22}\varepsilon_{2'2'},\\ &Q^{(k)}_{11}=\frac{E^{(k)}_1}{1-v^{(k)}_{12}v^{(k)}_{21}},\quad Q^{(k)}_{22}=\frac{E^{(k)}_2}{1-v^{(k)}_{12}v^{(k)}_{21}},\quad Q^{(k)}_{12}=\frac{v^{(k)}_{12}E^{(k)}_2}{1-v^{(k)}_{12}v^{(k)}_{21}}.\end{aligned} \tag{26}$$

Substituting further the tangential normal stresses from Eq. (26) into Eq. (24b) and solving for the transverse normal stress, one obtains

$$\begin{aligned}&S^{(k)}_{33}=Q^{(k)}_{13}\varepsilon_{1'1'}+Q^{(k)}_{23}\varepsilon_{2'2'}+Q^{(k)}_{33}\varepsilon_{33},\\ &Q^{(k)}_{13}=\frac{v^{(k)}_{13}+v^{(k)}_{12}v^{(k)}_{23}}{1-v^{(k)}_{12}v^{(k)}_{21}}E^{(k)}_3,\quad Q^{(k)}_{23}=\frac{v^{(k)}_{23}+v^{(k)}_{21}v^{(k)}_{13}}{1-v^{(k)}_{12}v^{(k)}_{21}}E^{(k)}_3,\quad Q^{(k)}_{33}=E^{(k)}_3.\end{aligned} \tag{27}$$

In coordinate directions α_1, α_2 and α_3 the equations of the constitutive law can be represented as Eqs. (23a)–(23c). For components of the elasticity tensor of the kth layer the following formulas are valid [16]:

$$
\begin{aligned}
&C^{(k)}_{1111} = Q^{(k)}_{11}\zeta_k^4 + 2\mu_k\xi_k^2\zeta_k^2 + Q^{(k)}_{22}\xi_k^4, \quad C^{(k)}_{2222} = Q^{(k)}_{11}\xi_k^4 + 2\mu_k\xi_k^2\zeta_k^2 + Q^{(k)}_{22}\zeta_k^4,\\
&C^{(k)}_{1122} = (Q^{(k)}_{11} + Q^{(k)}_{22} - 2\mu_k)\xi_k\zeta_k + Q^{(k)}_{12}, \quad C^{(k)}_{1212} = (Q^{(k)}_{11} + Q^{(k)}_{22} - 2\mu_k)\xi_k\zeta_k + G^{(k)}_{12},\\
&C^{(k)}_{1112} = (\mu_k - Q^{(k)}_{11})\xi_k\zeta_k^3 + (Q^{(k)}_{22} - \mu_k)\xi_k^3\zeta_k, \quad C^{(k)}_{2212} = (\mu_k - Q^{(k)}_{11})\xi_k^3\zeta_k + (Q^{(k)}_{22} - \mu_k)\xi_k\zeta_k^3,\\
&C^{(k)}_{3311} = Q^{(k)}_{13}\zeta_k^2 + Q^{(k)}_{23}\xi_k^2, \quad C^{(k)}_{3322} = Q^{(k)}_{13}\xi_k^2 + Q^{(k)}_{23}\zeta_k^2,\\
&C^{(k)}_{3312} = (Q^{(k)}_{23} - Q^{(k)}_{13})\xi_k\zeta_k, \quad C^{(k)}_{3333} = Q^{(k)}_{33},\\
&C^{(k)}_{1313} = G^{(k)}_{13}\zeta_k^2 + G^{(k)}_{23}\xi_k^2, \quad C^{(k)}_{2323} = G^{(k)}_{13}\xi_k^2 + G^{(k)}_{23}\zeta_k^2,\\
&C^{(k)}_{1323} = (G^{(k)}_{23} - G^{(k)}_{13})\xi_k\zeta_k, \quad \mu_k = Q^{(k)}_{12} + 2G^{(k)}_{12}, \quad \xi_k = \sin\gamma_k, \quad \zeta_k = \cos\gamma_k,
\end{aligned}
\tag{28}
$$

where γ_k is the angle between axes of symmetry $\alpha^{(k)}_{1'}$ and $\alpha^{(k)}_{2'}$ of the kth layer and coordinate directions α_1 and α_2.

In particular, for the multilayered isotropic shell we have

$$
\begin{aligned}
&C^{(k)}_{1111} = C^{(k)}_{2222} = \frac{E_k}{1-\nu_k^2}, \quad C^{(k)}_{3333} = E_k, \quad C^{(k)}_{1122} = \frac{\nu_k E_k}{1-\nu_k^2},\\
&C^{(k)}_{3311} = C^{(k)}_{3322} = \frac{\nu_k E_k}{1-\nu_k}, \quad C^{(k)}_{1212} = C^{(k)}_{1313} = C^{(k)}_{2323} = \frac{E_k}{2(1+\nu_k)},\\
&C^{(k)}_{1112} = C^{(k)}_{2212} = C^{(k)}_{3312} = C^{(k)}_{1323} = 0.
\end{aligned}
\tag{29}
$$

It should be mentioned that the proposed approach gives the possibility to use six-parameter shell model in conjunction with the assumed strain method without additional stabilization algorithms. No enhanced strains [4–6,12,26–28] are needed to obtain the solution of the bending dominated shell problems, and no Poisson thickness locking can occur when Poisson's ratios are not equal to zero. It will be discussed in Section 7.

6. FE formulation

The Hu–Washizu functional (16) for the element can be written in a matrix form:

$$
\begin{aligned}
&J^{e\ell} = \int_{-1}^{1}\int_{-1}^{1}\left[\tfrac{1}{2}\mathbf{E}^{\mathrm{T}}\mathbf{D}\mathbf{E} - \left(\mathbf{E}^{\mathrm{T}} - \mathbf{e}^{\mathrm{T}} - \boldsymbol{\eta}^{\mathrm{T}}\right)\mathbf{H} - \mathbf{v}^{\mathrm{T}}\mathbf{P}\right]\Lambda\,\mathrm{d}\xi_1\,\mathrm{d}\xi_2 - \oint_{\Gamma^{e\ell}}\mathbf{v}_\Gamma^{\mathrm{T}}\hat{\mathbf{H}}_\Gamma\bar{\gamma}\,\mathrm{d}s,\\
&\mathbf{H} = \left[\mathscr{H}^-_{11} \quad \mathscr{H}^+_{11} \quad \mathscr{H}^-_{22} \quad \mathscr{H}^+_{22} \quad \mathscr{H}^-_{12} \quad \mathscr{H}^+_{12} \quad \mathscr{H}^-_{13} \quad \mathscr{H}^+_{13} \quad \mathscr{H}^-_{23} \quad \mathscr{H}^+_{23} \quad \mathscr{H}_{33}\right]^{\mathrm{T}},\\
&\mathbf{E} = \left[E^-_{11} \quad E^+_{11} \quad E^-_{22} \quad E^+_{22} \quad E^-_{12} \quad E^+_{12} \quad E^-_{13} \quad E^+_{13} \quad E^-_{23} \quad E^+_{23} \quad E_{33}\right]^{\mathrm{T}},\\
&\mathbf{e} = \left[e^-_{11} \quad e^+_{11} \quad e^-_{22} \quad e^+_{22} \quad e^-_{12} \quad e^+_{12} \quad e^-_{13} \quad e^+_{13} \quad e^-_{23} \quad e^+_{23} \quad e_{33}\right]^{\mathrm{T}},\\
&\boldsymbol{\eta} = \left[\eta^-_{11} \quad \eta^+_{11} \quad \eta^-_{22} \quad \eta^+_{22} \quad \eta^-_{12} \quad \eta^+_{12} \quad \eta^-_{13} \quad \eta^+_{13} \quad \eta^-_{23} \quad \eta^+_{23} \quad \eta_{33}\right]^{\mathrm{T}},
\end{aligned}
\tag{30}
$$

where ξ_1 and ξ_2 are the local coordinates of the element; $\Lambda(\xi_1,\xi_2)$ is the function characterizing the metric of the element; $\mathbf{v} = [v_1^-\ v_1^+\ v_2^-\ v_2^+\ v_3^-\ v_3^+]^{\mathrm{T}}$ is the displacement vector; $\mathbf{v}_\Gamma = [v_\nu^-\ v_\nu^+\ v_t^-\ v_t^+\ v_3^-\ v_3^+]^{\mathrm{T}}$ is the displacement vector of the element edge $\Gamma^{e\ell}$; $\mathbf{E}$ is the strain vector; $\mathbf{e}$ and $\boldsymbol{\eta}$ are the linear and non-linear parts of the strain–displacement transformation vector; $\mathbf{H}$ is the stress resultant vector; $\hat{\mathbf{H}}_\Gamma = [\hat{\mathscr{H}}^-_{\nu\nu}\ \hat{\mathscr{H}}^+_{\nu\nu}\ \hat{\mathscr{H}}^-_{\nu t}\ \hat{\mathscr{H}}^+_{\nu t}\ \hat{\mathscr{H}}^-_{\nu 3}\ \hat{\mathscr{H}}^+_{\nu 3}]^{\mathrm{T}}$ is the loading resultant vector acting on the edge of the element; $\mathbf{P} = [-p_1^-\ p_1^+\ -p_2^-\ p_2^+\ -p_3^-\ p_3^+]^{\mathrm{T}}$ is the surface traction vector; $\mathbf{D}$ is the constitutive stiffness matrix of order 11×11, which components are defined by Eq. (19) in accordance with Ref. [20].

For the simplest quadrilateral four-node shell element the displacement field is approximated according to the standard C^0 interpolation

$$\mathbf{v} = \sum_n N_n \mathbf{v}_n, \tag{31}$$

where $\mathbf{v}_n = [v_{1n}^- \; v_{1n}^+ \; v_{2n}^- \; v_{2n}^+ \; v_{3n}^- \; v_{3n}^+]^{\mathrm{T}}$ are the displacement vectors of the element nodes; $N_n(\underline{\xi_1}, \underline{\xi_2})$ are the linear shape functions of the element; the index n denotes a number of nodes and equals $\overline{1,4}$. The load vector is also assumed to vary linearly inside the element.

According to the assumed strain concept developed by Hughes and Tezduyar [29], Wempner et al. [30], and Betsch and Stein [4], the following strain interpolations are adopted:

$$\mathbf{E} = \sum_{r_1,r_2} \mathbf{Q}^{r_1 r_2} \mathbf{E}^{r_1 r_2} \xi_1^{r_1} \xi_2^{r_2}. \tag{32}$$

Here,

$$\mathbf{E}^{00} = \begin{bmatrix} E_{11}^{-00} & E_{11}^{+00} & E_{22}^{-00} & E_{22}^{+00} & E_{12}^{-00} & E_{12}^{+00} & E_{13}^{-00} & E_{13}^{+00} & E_{23}^{-00} & E_{23}^{+00} & E_{33}^{00} \end{bmatrix}^{\mathrm{T}},$$

$$\mathbf{E}^{01} = \begin{bmatrix} E_{11}^{-01} & E_{11}^{+01} & E_{13}^{-01} & E_{13}^{+01} & E_{33}^{01} \end{bmatrix}^{\mathrm{T}}, \quad \mathbf{E}^{10} = \begin{bmatrix} E_{22}^{-10} & E_{22}^{+10} & E_{23}^{-10} & E_{23}^{+10} & E_{33}^{10} \end{bmatrix}^{\mathrm{T}}, \quad \mathbf{E}^{11} = [E_{33}^{11}],$$

$$\mathbf{Q}^{01} = \begin{bmatrix} 1&0&0&0&0 \\ 0&1&0&0&0 \\ 0&0&0&0&0 \\ 0&0&0&0&0 \\ 0&0&0&0&0 \\ 0&0&0&0&0 \\ 0&0&1&0&0 \\ 0&0&0&1&0 \\ 0&0&0&0&0 \\ 0&0&0&0&0 \\ 0&0&0&0&1 \end{bmatrix}, \quad \mathbf{Q}^{10} = \begin{bmatrix} 0&0&0&0&0 \\ 0&0&0&0&0 \\ 1&0&0&0&0 \\ 0&1&0&0&0 \\ 0&0&0&0&0 \\ 0&0&0&0&0 \\ 0&0&0&0&0 \\ 0&0&0&0&0 \\ 0&0&1&0&0 \\ 0&0&0&1&0 \\ 0&0&0&0&1 \end{bmatrix}, \quad \mathbf{Q}^{11} = \begin{bmatrix} 0 \\ 0 \\ 0 \\ 0 \\ 0 \\ 0 \\ 0 \\ 0 \\ 0 \\ 0 \\ 1 \end{bmatrix} \tag{33}$$

where $\mathbf{Q}^{00}$ is the identity matrix of order 11×11; $\mathbf{E}^{00}$ is the vector of homogeneous states of strains; $\mathbf{E}^{01}$, $\mathbf{E}^{10}$ and $\mathbf{E}^{11}$ are the vectors of higher approximation modes of strains. Throughout this section superscripts r_1 and r_2 take the values 0 and 1.

The interpolations of the stress resultants follow the forms of the conjugate strains

$$\mathbf{H} = \sum_{r_1,r_2} \mathbf{Q}^{r_1 r_2} \mathbf{H}^{r_1 r_2} \xi_1^{r_1} \xi_2^{r_2}, \tag{34}$$

where vectors $\mathbf{H}^{r_1 r_2}$ are defined by replacing a letter E by a letter $\mathscr{H}$ in Eq. (33).

Accounting for the strain–displacement relationships (17) and substituting Eqs. (31)–(34) into the functional (30), one can obtain using the standard variational procedure the governing equations of the present FE formulation

$$\mathbf{E}^{r_1 r_2} = (\mathbf{Q}^{r_1 r_2})^{\mathrm{T}} (\mathbf{B}^{r_1 r_2} + \mathbf{R}^{r_1 r_2} \mathbf{u}) \mathbf{u}, \tag{35a}$$

$$\mathbf{H}^{r_1 r_2} = (\mathbf{Q}^{r_1 r_2})^{\mathrm{T}} \mathbf{D} \mathbf{Q}^{r_1 r_2} \mathbf{E}^{r_1 r_2}, \tag{35b}$$

$$\sum_{r_1,r_2} \frac{1}{3^{r_1+r_2}} (\mathbf{B}^{r_1r_2} + 2\mathbf{R}^{r_1r_2}\mathbf{u})^{\mathrm{T}} \mathbf{Q}^{r_1r_2} \mathbf{H}^{r_1r_2} = \mathbf{F}, \tag{35c}$$

where $\mathbf{u} = [\mathbf{v}_1^{\mathrm{T}}\ \mathbf{v}_2^{\mathrm{T}}\ \mathbf{v}_3^{\mathrm{T}}\ \mathbf{v}_4^{\mathrm{T}}]^{\mathrm{T}}$ is the displacement vector at nodal points of the element; $\mathbf{F}$ is the force vector; $\mathbf{B}^{r_1r_2}$ are the matrices of order 11×24 corresponding to the linear strain–displacement transformation; $\mathbf{R}^{r_1r_2}$ are the 3-D arrays of order $11 \times 24 \times 24$ corresponding to the non-linear strain–displacement transformation. It is apparent that in Eqs. (35a) and (35c) $\mathbf{R}^{r_1r_2}\mathbf{u}$ imply matrices of order 11×24, and the following rule is used in calculations:

$$(\mathbf{R}^{r_1r_2}\mathbf{u})_{pq} = \sum_r R^{r_1r_2}_{pqr} u_r \quad (p = \overline{1,11} \text{ and } q, r = \overline{1,24}).$$

It is important to note that due to an approach developed in Ref. [19] the following coupling equations can be deduced from Eqs. (35a)–(35c):

$$\begin{aligned} hE^{10}_{33} &= A_1\bar{\zeta}_1(E^{+00}_{13} - E^{-00}_{13}), \quad hE^{01}_{33} = A_2\bar{\zeta}_2(E^{+00}_{23} - E^{-00}_{23}), \\ hE^{11}_{33} &= A_1\bar{\zeta}_1(E^{+01}_{13} - E^{-01}_{13}), \quad hE^{11}_{33} = A_2\bar{\zeta}_2(E^{+10}_{23} - E^{-10}_{23}). \end{aligned} \tag{36}$$

Relationships (36) imply that only seven higher approximation modes of strains are independent of 11 higher approximation modes from Eq. (33). This provides a correct rank of the elemental matrix [19]. It should be mentioned that all matrix calculations are evaluated by using the full exact analytical integration. So, our FE formulation is very economical and efficient.

Up to this moment, no incremental arguments are needed in the total Lagrangian formulation. The incremental displacements, strains and stress resultants are needed for solving non-linear Eqs. (35a)–(35c) on the basis of the Newton–Raphson method. Further, the left superscripts t and $t + \Delta t$ indicate in which configuration at time t or time $t + \Delta t$ a quantity occurs. Then, in accordance with this agreement we have

$${}^{t+\Delta t}\mathbf{E}^{r_1r_2} = {}^{t}\mathbf{E}^{r_1r_2} + \Delta\mathbf{E}^{r_1r_2}, \quad {}^{t+\Delta t}\mathbf{H}^{r_1r_2} = {}^{t}\mathbf{H}^{r_1r_2} + \Delta\mathbf{H}^{r_1r_2}, \quad {}^{t+\Delta t}\mathbf{u} = {}^{t}\mathbf{u} + \Delta\mathbf{u}, \quad {}^{t+\Delta t}\mathbf{F} = {}^{t}\mathbf{F} + \Delta\mathbf{F}, \tag{37}$$

where $\Delta\mathbf{E}^{r_1r_2}$, $\Delta\mathbf{H}^{r_1r_2}$, $\Delta\mathbf{u}$ and $\Delta\mathbf{F}$ are the incremental variables.

Substituting formulas (37) into Eqs. (35a)–(35c), and taking into account that the external loads and the second Piola–Kirchhoff stresses constitute the self-equilibrated system in the configuration at time t, one can obtain the following incremental equations:

$$\Delta\mathbf{E}^{r_1r_2} = (\mathbf{Q}^{r_1r_2})^{\mathrm{T}}({}^{t}\mathbf{M}^{r_1r_2} + \mathbf{R}^{r_1r_2}\Delta\mathbf{u})\Delta\mathbf{u}, \tag{38a}$$

$$\Delta\mathbf{H}^{r_1r_2} = (\mathbf{Q}^{r_1r_2})^{\mathrm{T}}\mathbf{D}\mathbf{Q}^{r_1r_2}\Delta\mathbf{E}^{r_1r_2}, \tag{38b}$$

$$\sum_{r_1,r_2} \frac{1}{3^{r_1+r_2}} \left[2(\mathbf{R}^{r_1r_2}\Delta\mathbf{u})^{\mathrm{T}}\mathbf{Q}^{r_1r_2}{}^{t}\mathbf{H}^{r_1r_2} + ({}^{t}\mathbf{M}^{r_1r_2} + 2\mathbf{R}^{r_1r_2}\Delta\mathbf{u})^{\mathrm{T}}\mathbf{Q}^{r_1r_2}\Delta\mathbf{H}^{r_1r_2}\right] = \Delta\mathbf{F}, \tag{38c}$$

where ${}^{t}\mathbf{M}^{r_1r_2}$ are the matrices of order 11×24 corresponding to the configuration at time t:

$${}^{t}\mathbf{M}^{r_1r_2} = \mathbf{B}^{r_1r_2} + 2\mathbf{R}^{r_1r_2}{}^{t}\mathbf{u}.$$

Eliminating incremental strains and incremental stress resultants from Eqs. (38a)–(38c) and introducing matrices of order 11×11

$$\mathbf{D}^{r_1r_2} = \mathbf{Q}^{r_1r_2}(\mathbf{Q}^{r_1r_2})^{\mathrm{T}}\mathbf{D}\mathbf{Q}^{r_1r_2}(\mathbf{Q}^{r_1r_2})^{\mathrm{T}},$$

one obtains the governing incremental equilibrium equations

$$\mathbf{G}(\Delta\mathbf{u}) = \Delta\mathbf{F}, \tag{39a}$$

where

$$\mathbf{G}(\Delta\mathbf{u}) = \sum_{r_1,r_2} \frac{1}{3^{r_1+r_2}} \left[2(\mathbf{R}^{r_1r_2}\Delta\mathbf{u})^{\mathrm{T}}\mathbf{Q}^{r_1r_2}\,{}^{t}\mathbf{H}^{r_1r_2} + ({}^{t}\mathbf{M}^{r_1r_2} + 2\mathbf{R}^{r_1r_2}\Delta\mathbf{u})^{\mathrm{T}}\mathbf{D}^{r_1r_2}({}^{t}\mathbf{M}^{r_1r_2} + \mathbf{R}^{r_1r_2}\Delta\mathbf{u})\Delta\mathbf{u} \right]. \tag{39b}$$

Due to the existence of non-linear terms in Eq. (39a), the Newton–Raphson iteration process should be employed to solve these equations

$$\Delta\mathbf{u}^{[n+1]} = \Delta\mathbf{u}^{[n]} + \left[\frac{\partial\mathbf{G}}{\partial\Delta\mathbf{u}}(\Delta\mathbf{u}^{[n]}) \right]^{-1} \left[\Delta\mathbf{F} - \mathbf{G}(\Delta\mathbf{u}^{[n]}) \right], \tag{40}$$

where $n = 0, 1, \ldots$

The equilibrium equations (40) for each element are assembled by the usual technique to form the global incremental equilibrium equations. These incremental equations should be performed until the required accuracy of the solution can be obtained. The convergence criterion used herein can be described as

$$\left\| \Delta\mathbf{U}^{[n+1]} - \Delta\mathbf{U}^{[n]} \right\| < \varepsilon \left\| \Delta\mathbf{U}^{[n]} \right\|, \tag{41}$$

where $\| \bullet \|$ stands for the Euclidean norm in the displacement space; $\Delta\mathbf{U}$ is the global vector of displacement increments; ε is the priori chosen tolerance.

7. Numerical tests

To assess the accuracy and effectiveness of the developed TM shell elements TMS4c (complete stress–strain equations (21) are used) and TMS4r (modified stress–strain equations (23) are used), a standard linear pinched hemispherical shell test and five tests concerning homogeneous and composite beams, plates and shells undergoing finite rotations were employed. In all non-linear tests the tolerance error from criterion (41) is set to be $\varepsilon = 10^{-6}$.

The computations were performed on a standard PC Pentium/600. It should be also mentioned that no difference between both TMS4r and TMS4c elements can be observed when Poisson's ratios are equal to zero.

7.1. Pinched hemispherical shell

To illustrate the capability of the developed TMS4r and TMS4c elements to overcome membrane and shear locking phenomena and to compare their with the high performance four-node quadrilateral elements [36–40], we consider one of the most demanding standard linear test. A hemispherical shell with 18° hole at the top is loaded by two pairs of opposite concentrated forces on the equator. The geometrical and material data of the problem are shown in Fig. 4(a). In spite of the relatively small loading factor $f = 0.1$, it is a large rotation problem because the shell response to the pinching load is dominated by rigid-body rotations about normals to the reference surface.

Due to symmetry of the problem, only one quarter of the shell is modeled with regular meshes of the TMS4 elements. Table 1 lists a comparison of the normalized displacement under an applied load between the TMS4 elements and above four-node quadrilateral elements extracted from the literature in Ref. [41]. The displacements are normalized with respect to the value of 0.0940 [41], while our displacement is normalized with respect to the value of 0.0935. Such a value is the computationally exact solution of this problem based on the developed TM shell theory. It is seen that our results show an excellent agreement even for coarse meshes.

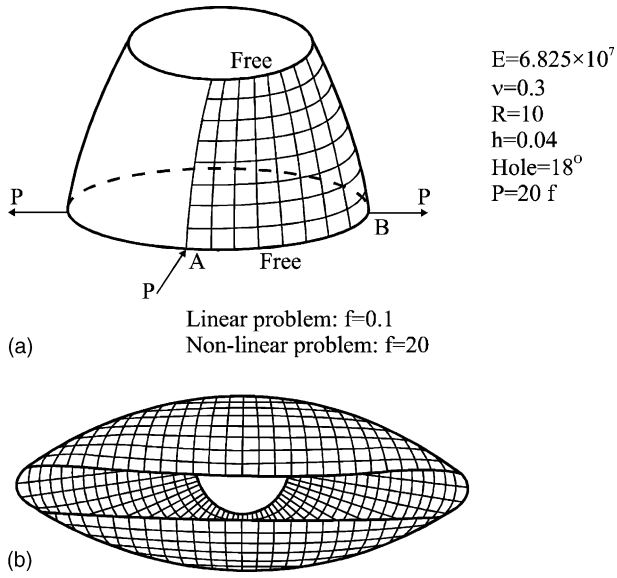

Fig. 4. Pinched hemispherical shell: (a) geometry and (b) deformed configuration for the loading factor $f = 20$.

Table 1
Pinched hemispherical shell. Linear solution for the normalized transverse displacement under an applied load ($f = 0.1$)

Mesh	SRI [36]	RSDS [37]	MITC4 [38]	Mixed [39]	QPH [40]	TMS4r	TMS4c
4×4	0.412	0.965	0.390	0.651	0.280	0.878	0.869
8×8	0.927	0.971	0.910	0.968	0.860	0.956	0.952
16×16	0.984	0.989	0.989	0.993	0.990	0.985	0.982
32×32						0.996	0.992

For the non-linear calculations we have chosen the loading factor $f = 20$. Table 2 and Fig. 5 present a comparison with solutions reported in Refs. [6,11]. In Table 2 a number of used loading steps of the equal magnitude for the different meshes and loading factor $f = 20$ is also shown. As can be seen, the developed TMS4 elements perform very well. It is important to note that, when we used 10 loading steps to determine a shell response, the results were *exactly* the same but the final number of iterations was almost twice more. Additionally, the deformed configuration of the hemisphere is displayed in Fig. 4(b).

Table 2
Pinched hemispherical shell. Non-linear solution for the transverse displacement $\bar{v}_3 = (v_3^- + v_3^+)/2$ under applied loads

Element	Mesh	$f = 10$		$f = 20$		
		$-\bar{v}_3^A$	$\bar{v}_3^B$	$-\bar{v}_3^A$	$\bar{v}_3^B$	Number of loading steps
2-D shell [11]		5.867	3.408	8.148	4.073	
3-D shell [11]		5.549	3.292	7.728	3.959	
TMS4r	16×16	5.790	3.378	8.136	4.054	4
	32×32	5.836	3.398	8.137	4.067	5
	64×64	5.852	3.404	8.142	4.072	4
TMS4c	16×16	5.476	3.260	7.696	3.935	4
	32×32	5.528	3.282	7.717	3.951	5
	64×64	5.547	3.291	7.730	3.958	4

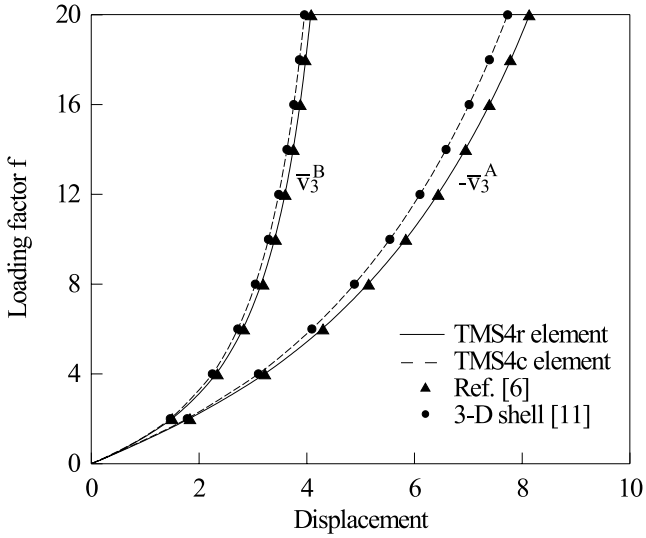

Fig. 5. Displacement $\bar{v}_3 = (v_3^- + v_3^+)/2$ of the hemispherical shell.

The results from Fig. 5 also illustrate the sensitivity of the TMS4 elements to Poisson thickness locking [27,28]. As pointed out already, Poisson thickness locking occurs in bending dominated problems when Poisson's ratio is not equal to zero. One can see that our refined TMS4r element is completely free from the Poisson locking phenomenon.

7.2. Cantilever beam under two pairs of tip forces

This numerical example demonstrates the ability of our FE formulation to represent adequately x_1x_3 in-plane beam bending as well as x_1x_2 in-plane beam bending. For this purpose we consider a beam with the square cross-section subjected to two pairs of tip forces as shown in Fig. 6. So, two different types of loading displayed in Fig. 6(a) and (b) need to be investigated. Note that we were not interested in exact results, only the difference between the aforementioned problems was important.

Table 3 lists the results of solving both beam problems by using the 20×1 mesh of TMS4r elements. One can observe that corresponding results are exactly the same. It seems that our TMS4r element performs well. It is important that all results have been obtained by using *only one* loading step and further loading is

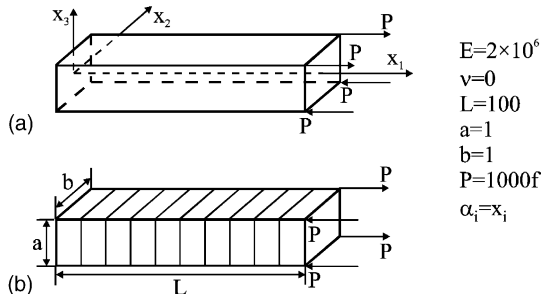

Fig. 6. Cantilever beam under two pairs of tip forces: (a) x_1x_3 in-plane bending and (b) x_1x_2 in-plane bending.

Table 3
Tip displacements $\bar{v}_i = (v_i^- + v_i^+)/2$ of the centerline of the cantilever beam under two pairs of tip forces

Element	Loading factor f	x_1x_3 in-plane bending			x_1x_2 in-plane bending		
		$-\bar{v}_1$	$-\bar{v}_3$	Number of iterations	$-\bar{v}_1$	$-\bar{v}_2$	Number of iterations
TMS4r	1	10.82	38.74	13	10.82	38.74	13
	3	23.18	53.96	21	23.18	53.96	21
	5	27.55	57.73	30	27.55	57.73	30

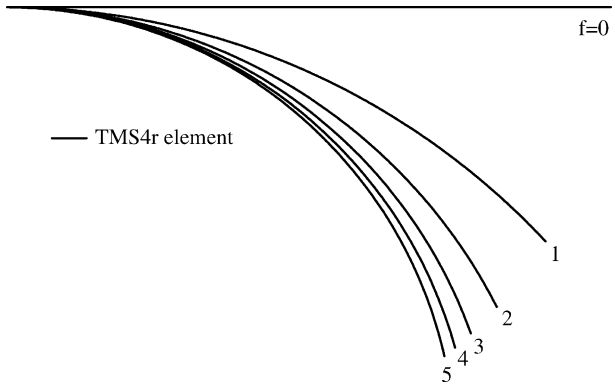

Fig. 7. Deformed configurations of the cantilever beam: x_1x_3 in-plane bending.

possible. In this problem we did not discover an escape of the initial trial value from Newton's attraction area for all reasonable levels of loading. For a complete picture Fig. 7 presents five deformed beam configurations for x_1x_3 in-plane bending.

7.3. Cantilever curved beam under two pairs of tip forces

Let us consider a cantilever curved beam whose centerline is one octant of the circle lying in the x_1x_2 plane. The beam is subjected to conservative tip loads in the x_3 direction. The geometrical and material data of the problem are given in Fig. 8. It was selected in order to test a sensitivity of the curved beam response to different types of structure geometry (see for the comparison Fig. 8(a) and (b)).

Table 4 lists the results reported in Refs. [42–46] using eight straight elements and extracted from the literature in Ref. [47]. Our results have been obtained by modeling a structure with the 1×8 mesh of TMS4r elements for both problems. It should be noted that all results have been calculated by using *only one* loading step including the last level of loading $Q = 2400$. In this problem we did not also discover an escape of the initial trial value from Newton's attractive area for all reasonable levels of loading for the developed shell element as well as the plate element.

7.4. Cantilever cross-ply cylindrical segment under tip load

This problem was presented in Ref. [48] for testing the non-linear shell element and further has been used as a benchmark test for the non-linear behaviour of the 3-D shell element in Ref. [24]. The geometrical and

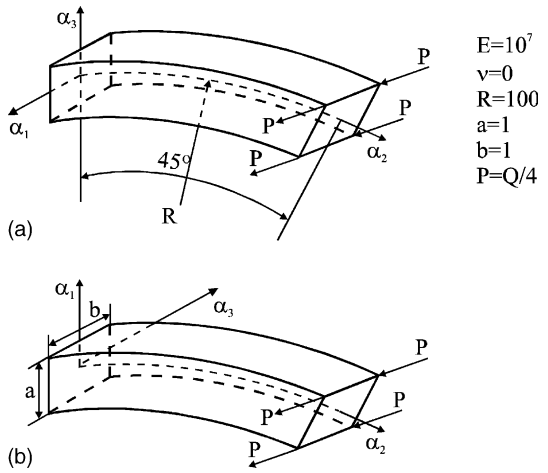

Fig. 8. Cantilever curved beam under two pairs of tip forces: (a) cylindrical shell ($k_1 = 0$, $k_2 = 1/R$) and (b) ring plate ($k_1 = 0$, $k_2 = 0$).

Table 4
Tip point coordinates of the centerline of the cantilever curved beam under two pairs of tip forces

Element	$Q = 300$			$Q = 600$			$Q = 2400$		
	x_1	x_2	x_3	x_1	x_2	x_3	x_1	x_2	x_3
Ref. [42]	22.5	59.2	39.5	15.9	47.2	53.4			
Ref. [43]	22.33	58.84	40.08	15.79	47.23	53.37			
Ref. [44]	22.14	58.64	40.35	15.55	47.04	53.50			
Ref. [45]	22.16	58.53	40.53	15.61	47.64	53.71			
Ref. [46]	22.31	58.85	40.08	15.75	47.25	53.37			
Ref. [47]	22.67	58.51	40.14	16.39	46.73	53.33			
TMS4r (shell)	22.25	58.79	40.25	15.62	47.03	53.64	5.104	25.23	67.54
TMS4r (plate)	22.25	58.79	40.25	15.62	47.03	53.64	5.104	25.23	67.54

material characteristics of the three-layer cylindrical segment are given in Fig. 9, where R^{inner} denotes the inner radius of the shell, subscripts L and T refer to the longitudinal and transverse directions of the individual ply, and 0° and 90° refer to the axial and circumferential directions of the cylinder.

Due to symmetry of the problem, only half of the shell is discretized with the 16×16 mesh of TMS4 elements. Fig. 10 displays the dependence of the displacement $\bar{v}_3 = (v_3^- + v_3^+)/2$ under the applied load on the loading factor f for different ply orientations and the comparison with results reported in Refs. [24,48] for the $[0/90/0]$ laminate using the four-node degenerate shell element and eight-node brick-type shell element, respectively. One can see that all elements perform well but our TMS4r and TMS4c elements are less expensive, since all calculations are evaluated applying the full exact analytical integration; no inversion is needed if an element is rectangular. Note that our results have been obtained again by using *only one* loading step and further loading is possible.

7.5. Clamped angle-ply cylindrical panel under center point load

This numerical example has been treated in Ref. [49] for testing the non-linear anisotropic shell element behaviour. It is assumed that the curved edges are free while the straight edges are clamped. The geo-

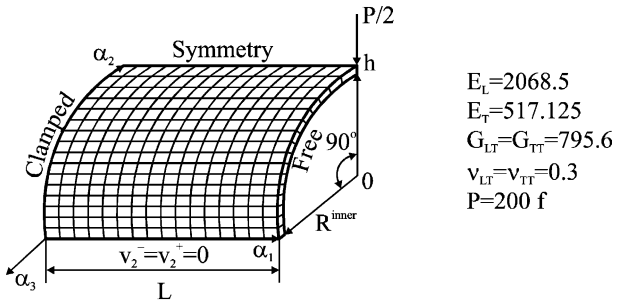

L=304.8, R^{inner}=100.1, h=3, Ply thickness=1
Ply orientation=[90/0/0], [0/90/0] and [0/0/90]

Fig. 9. Cantilever cross-ply cylindrical segment under the tip load.

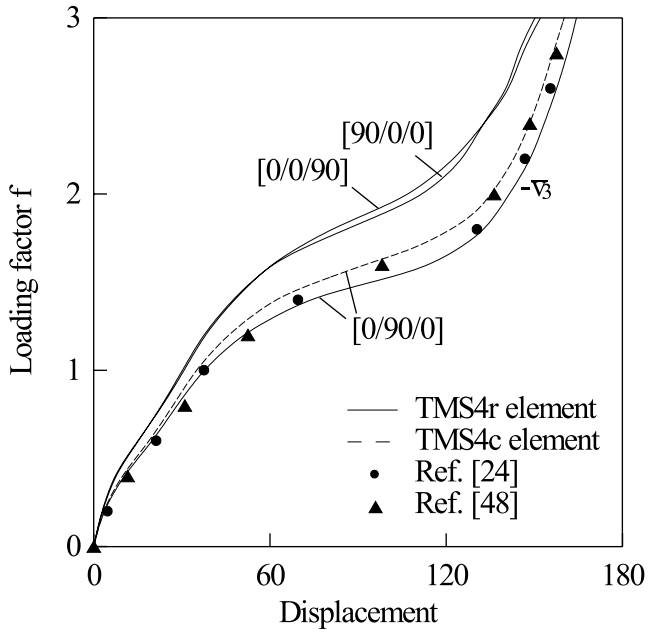

Fig. 10. Displacement $\bar{v}_3 = (v_3^- + v_3^+)/2$ of the cross-ply cylindrical segment under the applied load.

metrical and material data of the two-layer angle-ply cylindrical panel are shown in Fig. 11. Three different laminates were tested. The ply angle is measured in the clockwise direction from α_1 to the fiber direction.

Due to the anisotropic shell response, no symmetry conditions were used. We modeled the whole shell by using the 12×12 mesh of TMS4 elements. Fig. 12 displays the load-displacement curves for the center point of the middle surface for different ply orientations and the comparison with results reported in Ref. [49] for the $[45/-45]$ panel by using the 6×6 mesh of 9-node degenerate shell elements. It is seen that all results agree closely.

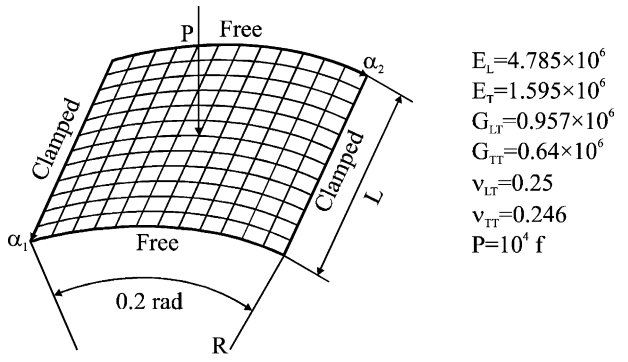

L=20, R=100, h=0.496, Ply thickness=0.248
Ply orientation=[15/-15], [45/-45] and [75/-75]

Fig. 11. Clamped angle-ply cylindrical panel under center point load.

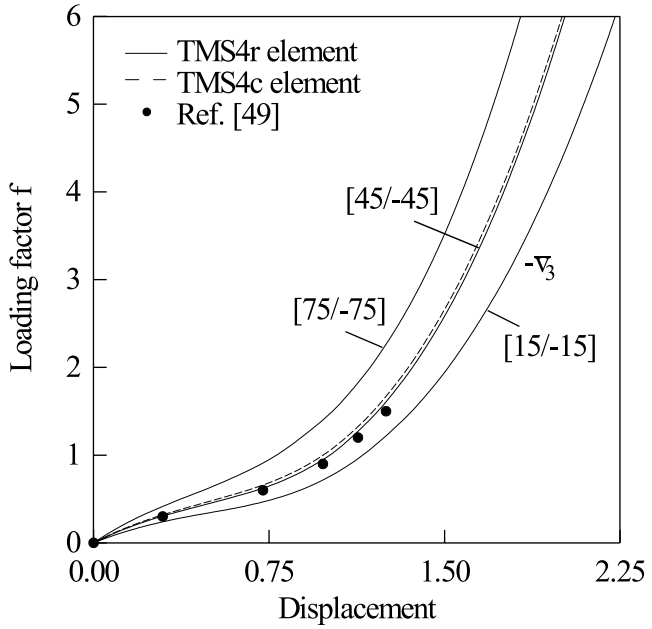

Fig. 12. Displacement $\bar{v}_3 = (v_3^- + v_3^+)/2$ of the angle-ply cylindrical panel under the applied load.

8. Conclusions

The simple and efficient mixed FE model has been developed for the analysis of TM shells undergoing finite deformations. The FE formulation is based on the non-linear strain–displacement equations that exactly represent the arbitrarily large rigid-body motions. As fundamental unknowns six displacements and 11 strains of the face surfaces, and 11 stress resultants have been chosen. This allows special loading conditions at the face surfaces and shell edges as in Sections 7.2 and 7.3 to be accounted for.

The proposed TM shell theory is free of assumptions of small displacements, small rotations and small loading steps because in this paper the *exact* theory based on the objective fully non-linear strain–displacement relationships has been developed. There exists only one limitation that a loading step cannot be too large. This restriction arises in the case of using the Newton–Raphson method, since the iteration process can be diverged due to an escape of the trial initial value from Newton's attractive area. Besides, the solution of our exact shell theory will be *unique* in a sense that it is independent on loading steps as well as a loading path.

As a result, the simplest quadrilateral four-node shell elements on the basis of the assumed strain concept can be used without special stabilization algorithms. The element characteristic arrays have been obtained by applying the Hu–Washizu mixed variational principle in conjunction with the incremental total Lagrangian formulation and Newton–Raphson method. The incremental total Lagrangian formulation has been used because, first, there is a natural undeformed state to which the deformed shell would return when it is unloaded, and, second, there are fully non-linear strain–displacement equations (5) exactly representing large rigid-body motions.

All matrix calculations are evaluated using the full exact analytical integration. So, our FE formulation is very economical and efficient. The developed TMS4r and TMS4c elements do not contain any spurious zero energy modes and possess a proper rank. An important feature of the proposed formulation is that no enhanced strains are needed to obtain the computationally exact solutions of the bending dominated shell problems and no Poisson thickness locking can occur when one uses our TMS4r element.

To demonstrate the accuracy and efficiency of the TMS4 elements, five tests for homogeneous and composite beams, plates and shells under conservative loading were employed. In all investigated problems the developed elements especially TMS4r element exhibited excellent performance. All our results excepting the pinched hemisphere were obtained by using *only one* loading step for the extremely large levels of loading and further loading is possible.

The extension to the layer-wise TM theory [35] of composite shells undergoing finite deformations poses no additional difficulties but requires algebra and computational efforts. This problem is currently under development.

Acknowledgements

This work was supported by Research Programs of Tambov State Technical University (grant no. 1Г/00–10) and Moscow State Technical University (MAMI) (grant no. 1.5.00).

We wish to thank the reviewer for his suggestions, which helped to improve a paper.

Appendix A

Consider a TM shell undergoing finite deformations. For the sake of convenience, the time variable is used to describe configurations of the shell under applied loading. In this connection the following notation is used to denote various shell configurations (see Fig. 13): ${}^0\boldsymbol{m}$ is the initial configuration at time t_0; ${}^t\boldsymbol{m}$ is the current configuration at time t; ${}^{t+\Delta t}\boldsymbol{m}$ is the final configuration at time $t+\Delta t$, where Δt is the time increment.

The position vectors depicted in Fig. 13 can be defined as functions of the orthogonal curvilinear coordinates in the initial shell configuration and the time variable, i.e.,

$$ {}^0\mathbf{R} = \mathbf{R}(\alpha_1, \alpha_2, \alpha_3, t_0), \quad {}^t\mathbf{R} = \mathbf{R}(\alpha_1, \alpha_2, \alpha_3, t), \quad {}^{t+\Delta t}\mathbf{R} = \mathbf{R}(\alpha_1, \alpha_2, \alpha_3, t+\Delta t). \tag{A.1} $$

The displacement vectors in configurations ${}^t\boldsymbol{m}$ and ${}^{t+\Delta t}\boldsymbol{m}$ according to the refined Timoshenko kinematic hypothesis (2) and presentations (A.1) are

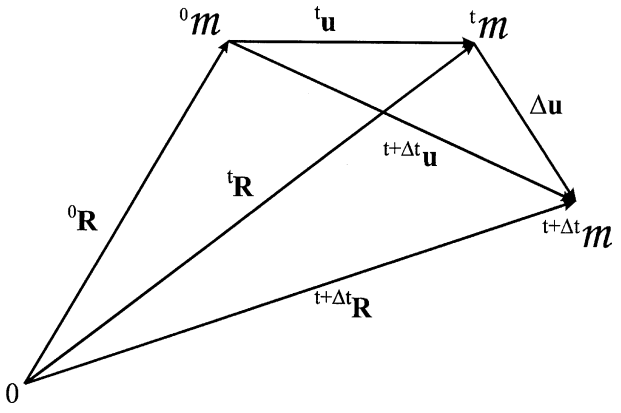

Fig. 13. Shell configurations.

$$ {}^{t}\mathbf{u} = {}^{t}\mathbf{R} - {}^{0}\mathbf{R} = N^{-}(\alpha_3)\,{}^{t}\mathbf{v}^{-} + N^{+}(\alpha_3)\,{}^{t}\mathbf{v}^{+}, \tag{A.2a} $$

$$ {}^{t+\Delta t}\mathbf{u} = {}^{t+\Delta t}\mathbf{R} - {}^{0}\mathbf{R} = N^{-}(\alpha_3)\,{}^{t+\Delta t}\mathbf{v}^{-} + N^{+}(\alpha_3)\,{}^{t+\Delta t}\mathbf{v}^{+}, \tag{A.2b} $$

where ${}^{t}\mathbf{v}^{\pm}$ and ${}^{t+\Delta t}\mathbf{v}^{\pm}$ are the displacement vectors of the face surfaces ${}^{t}S^{\pm}$ and ${}^{t+\Delta t}S^{\pm}$, respectively. Thus, for the displacement increment one can derive the following expression:

$$ \Delta\mathbf{u} = {}^{t+\Delta t}\mathbf{u} - {}^{t}\mathbf{u} = N^{-}(\alpha_3)\Delta\mathbf{v}^{-} + N^{+}(\alpha_3)\Delta\mathbf{v}^{+}, \tag{A.2c} $$

where $\Delta\mathbf{v}^{\pm} = {}^{t+\Delta t}\mathbf{v}^{\pm} - {}^{t}\mathbf{v}^{\pm}$ are the displacement increments of the face surfaces of the shell.

Allowing for Eq. (A.2) the incremental Green–Lagrange strain tensor (5) for the finite deformation TM shell analysis

$$ \Delta\varepsilon_{ij} = {}^{t+\Delta t}\varepsilon^{c}_{ij} - {}^{t}\varepsilon^{c}_{ij} \tag{A.3} $$

can be written in a vector form as

$$ \begin{aligned} 2\Delta\varepsilon_{\alpha\beta} = {} & N^{-}(\alpha_3)\left[\frac{1}{H^{-}_{\alpha}}\Delta\mathbf{v}^{-}_{,\alpha}\mathbf{e}_{\beta} + \frac{1}{H^{-}_{\beta}}\Delta\mathbf{v}^{-}_{,\beta}\mathbf{e}_{\alpha} + \frac{1}{H^{-}_{\alpha}H^{-}_{\beta}}\left({}^{t}\mathbf{v}^{-}_{,\alpha}\Delta\mathbf{v}^{-}_{,\beta} + {}^{t}\mathbf{v}^{-}_{,\beta}\Delta\mathbf{v}^{-}_{,\alpha} + \Delta\mathbf{v}^{-}_{,\alpha}\Delta\mathbf{v}^{-}_{,\beta}\right)\right] \\ & + N^{+}(\alpha_3)\left[\frac{1}{H^{+}_{\alpha}}\Delta\mathbf{v}^{+}_{,\alpha}\mathbf{e}_{\beta} + \frac{1}{H^{+}_{\beta}}\Delta\mathbf{v}^{+}_{,\beta}\mathbf{e}_{\alpha} + \frac{1}{H^{+}_{\alpha}H^{+}_{\beta}}\left({}^{t}\mathbf{v}^{+}_{,\alpha}\Delta\mathbf{v}^{+}_{,\beta} + {}^{t}\mathbf{v}^{+}_{,\beta}\Delta\mathbf{v}^{+}_{,\alpha} + \Delta\mathbf{v}^{+}_{,\alpha}\Delta\mathbf{v}^{+}_{,\beta}\right)\right], \end{aligned} \tag{A.4a} $$

$$ 2\Delta\varepsilon_{\alpha 3} = \Delta\boldsymbol{\beta}\mathbf{e}_{\alpha} + \frac{1}{\overline{H}_{\alpha}}\left(\Delta\bar{\mathbf{v}}_{,\alpha}\mathbf{e}_3 + {}^{t}\bar{\mathbf{v}}_{,\alpha}\Delta\boldsymbol{\beta} + {}^{t}\boldsymbol{\beta}\,\Delta\bar{\mathbf{v}}_{,\alpha} + \Delta\boldsymbol{\beta}\,\Delta\bar{\mathbf{v}}_{,\alpha}\right) + \frac{1}{\overline{H}_{\alpha}}(\alpha_3 - \bar{\delta})\Delta\varepsilon_{33,\alpha}, \tag{A.4b} $$

$$ \Delta\varepsilon_{33} = \Delta\boldsymbol{\beta}\mathbf{e}_3 + {}^{t}\boldsymbol{\beta}\,\Delta\boldsymbol{\beta} + \frac{1}{2}\Delta\boldsymbol{\beta}\,\Delta\boldsymbol{\beta}, \tag{A.4c} $$

$$ {}^{t}\boldsymbol{\beta} = \frac{1}{h}({}^{t}\mathbf{v}^{+} - {}^{t}\mathbf{v}^{-}), \quad \Delta\boldsymbol{\beta} = \frac{1}{h}(\Delta\mathbf{v}^{+} - \Delta\mathbf{v}^{-}), \tag{A.4d} $$

$$ {}^{t}\bar{\mathbf{v}} = \tfrac{1}{2}({}^{t}\mathbf{v}^{-} + {}^{t}\mathbf{v}^{+}), \quad \Delta\bar{\mathbf{v}} = \tfrac{1}{2}(\Delta\mathbf{v}^{-} + \Delta\mathbf{v}^{+}). \tag{A.4e} $$

Consider a shell in its current *deformed* configuration ${}^t\boldsymbol{m}$ and assume that it is further subjected to a large rigid-body motion from time t to time $t+\Delta t$. Then arbitrarily large rigid-body motions of the face surfaces of the shell can be represented in the following form:

$$\Delta\mathbf{v}^{\pm\mathrm{Rigid}} = {}^t\boldsymbol{\Delta} + ({}^t\mathbf{A} - \mathbf{E}){}^t\mathbf{R}^{\pm}, \tag{A.5a}$$

$${}^t\mathbf{R}^{\pm} = {}^0\mathbf{R}^{\pm} + {}^t\mathbf{v}^{\pm} = {}^0\mathbf{r} + \delta^{\pm}\mathbf{e}_3 + {}^t\mathbf{v}^{\pm}, \tag{A.5b}$$

where ${}^0\mathbf{r}$ is the position vector of any point of the reference surface in the initial configuration ${}^0\boldsymbol{m}$; ${}^t\boldsymbol{\Delta}$ is the constant displacement (translation) vector; ${}^t\mathbf{A}$ is the orthogonal matrix that defines a rigid-body rotation from time t to time $t+\Delta t$; $\mathbf{E}$ is the identity matrix.

The derivatives of the incremental displacements in accordance with Eqs. (11) and (A.5) will be

$$\Delta\mathbf{v}^{\pm\mathrm{Rigid}}_{,\alpha} = H^{\pm}_{\alpha}({}^t\mathbf{A}\mathbf{e}_{\alpha} - \mathbf{e}_{\alpha}) + {}^t\mathbf{A}\,{}^t\mathbf{v}^{\pm}_{,\alpha} - {}^t\mathbf{v}^{\pm}_{,\alpha}. \tag{A.6}$$

It can be verified by using Eqs. (A.5) and (A.6) that incremental strains from relationships (A.4) are *invariant* under large rigid body motions, i.e.,

$$\begin{aligned} 2\Delta\varepsilon^{\mathrm{Rigid}}_{\alpha\beta} &= \mathscr{P}({}^t\mathbf{A},\mathbf{e}_{\alpha},\mathbf{e}_{\beta}) + N^{-}(\alpha_3)\left[\frac{1}{H^{-}_{\alpha}}\mathscr{P}({}^t\mathbf{A},{}^t\mathbf{v}^{-}_{,\alpha},\mathbf{e}_{\beta}) + \frac{1}{H^{-}_{\beta}}\mathscr{P}({}^t\mathbf{A},{}^t\mathbf{v}^{-}_{,\beta},\mathbf{e}_{\alpha}) + \frac{1}{H^{-}_{\alpha}H^{-}_{\beta}}\mathscr{P}({}^t\mathbf{A},{}^t\mathbf{v}^{-}_{,\alpha},{}^t\mathbf{v}^{-}_{,\beta})\right] \\ &\quad + N^{+}(\alpha_3)\left[\frac{1}{H^{+}_{\alpha}}\mathscr{P}({}^t\mathbf{A},{}^t\mathbf{v}^{+}_{,\alpha},\mathbf{e}_{\beta}) + \frac{1}{H^{+}_{\beta}}\mathscr{P}({}^t\mathbf{A},{}^t\mathbf{v}^{+}_{,\beta},\mathbf{e}_{\alpha}) + \frac{1}{H^{+}_{\alpha}H^{+}_{\beta}}\mathscr{P}({}^t\mathbf{A},{}^t\mathbf{v}^{+}_{,\alpha},{}^t\mathbf{v}^{+}_{,\beta})\right] = 0, \end{aligned} \tag{A.7a}$$

$$\begin{aligned} 2\Delta\varepsilon^{\mathrm{Rigid}}_{\alpha 3} &= \frac{H_{\alpha}}{\overline{H}_{\alpha}}\left[\mathscr{P}({}^t\mathbf{A},\mathbf{e}_{\alpha},\mathbf{e}_3) + \mathscr{P}({}^t\mathbf{A},{}^t\boldsymbol{\beta},\mathbf{e}_{\alpha})\right] + \frac{1}{\overline{H}_{\alpha}}\left[\mathscr{P}({}^t\mathbf{A},{}^t\bar{\mathbf{v}}_{,\alpha},\mathbf{e}_3) + \mathscr{P}({}^t\mathbf{A},{}^t\bar{\mathbf{v}}_{,\alpha},{}^t\boldsymbol{\beta})\right] \\ &\quad + \frac{\alpha_3 - \bar{\delta}}{\overline{H}_{\alpha}}\left[\mathscr{P}({}^t\mathbf{A},{}^t\boldsymbol{\beta}_{,\alpha},\mathbf{e}_3) + \mathscr{P}({}^t\mathbf{A},{}^t\boldsymbol{\beta},{}^t\boldsymbol{\beta}_{,\alpha})\right] = 0, \end{aligned} \tag{A.7b}$$

$$2\Delta\varepsilon^{\mathrm{Rigid}}_{33} = \mathscr{P}({}^t\mathbf{A},\mathbf{e}_3,\mathbf{e}_3) + 2\mathscr{P}({}^t\mathbf{A},{}^t\boldsymbol{\beta},\mathbf{e}_3) + \mathscr{P}({}^t\mathbf{A},{}^t\boldsymbol{\beta},{}^t\boldsymbol{\beta}) = 0. \tag{A.7c}$$

The transformation $\mathscr{P}$ in Eq. (A.7) is introduced for convenience and defined as

$$\mathscr{P}(\mathbf{L},\mathbf{a},\mathbf{b}) = (\mathbf{L}\mathbf{a})(\mathbf{L}\mathbf{b}) - \mathbf{a}\mathbf{b},$$

where $\mathbf{L}$ is the matrix of order 3×3; $\mathbf{a}$ and $\mathbf{b}$ are the vectors of order 3; $(\mathbf{L}\mathbf{a})(\mathbf{L}\mathbf{b})$ and $\mathbf{a}\mathbf{b}$ denote the scalar products of the vectors. Note that due to the orthogonality property of the rotation matrix ${}^t\mathbf{A}$, an equality

$$\mathscr{P}({}^t\mathbf{A},\mathbf{a},\mathbf{b}) = 0$$

is valid for every pair of vectors.

References

[1] A. Barut, E. Madenci, A. Tessler, Nonlinear analysis of laminates through a Mindlin-type shear deformable shallow shell element, Comput. Meth. Appl. Mech. Engrg. 143 (1997) 155–173.

[2] Y. Basar, Y. Ding, R. Schultz, Refined shear-deformation models for composite laminates with finite rotations, Int. J. Solids Struct. 30 (1993) 2611–2638.

[3] K.J. Bathe, Finite Element Procedures, Prentice Hall, NJ, 1996.

[4] P. Betsch, E. Stein, An assumed strain approach avoiding artificial thickness straining for a nonlinear 4-node shell element, Commun. Numer. Meth. Engrg. 11 (1995) 899–909.

[5] M. Bischoff, E. Ramm, Shear deformable shell elements for large strains and rotations, Int. J. Numer. Meth. Engrg. 40 (1997) 4427–4449.

[6] N. Büchter, E. Ramm, Shell theory versus degeneration—a comparison in large rotation finite element analysis, Int. J. Numer. Meth. Engrg. 34 (1992) 39–59.
[7] M.A. Crisfield et al., Some aspects of the non-linear finite element method, Finite Elem. Anal. Design 27 (1997) 19–40.
[8] G. Horrigmoe, P.G. Bergan, Nonlinear analysis of free-form shells by flat finite elements, Comput. Meth. Appl. Mech. Engrg. 16 (1978) 11–35.
[9] T.J.R. Hughes, E. Carnoy, Non-linear finite element shell formulation accounting for large membrane strains, Comput. Meth. Appl. Mech. Engrg. 39 (1983) 69–82.
[10] I. Kreja, R. Schmidt, J.N. Reddy, Finite elements based on a first-order shear deformation moderate rotation shell theory with applications to the analysis of composite structures, Int. J. Non-Linear Mech. 32 (1997) 1123–1142.
[11] M. Li, F. Zhan, The finite deformation theory for beam, plate and shell. Part IV. The FE formulation of Mindlin plate and shell based on Green–Lagrangian strain, Comput. Meth. Appl. Mech. Engrg. 182 (2000) 187–203.
[12] J.C. Simo, F. Armero, Geometrically non-linear enhanced strain mixed methods and the method of incompatible modes, Int. J. Numer. Meth. Engrg. 33 (1992) 1413–1449.
[13] J.C. Simo, M.S. Rifai, D.D. Fox, On a stress resultant geometrically exact shell model. Part IV. Variable thickness shells with through-the-thickness stretching, Comput. Meth. Appl. Mech. Engrg. 81 (1990) 91–126.
[14] G.M. Stanley, K.S. Park, T.J.R. Hughes, Continuum-based resultant shell elements, in: T.J.R. Hughes, E. Hinton (Eds.), Finite Elem. Meth. Plate Shell Struct., Pineridge Press, Swansea, 1986, pp. 1–45.
[15] C.W.S. To, B. Wang, Hybrid strain based geometrically nonlinear laminated composite triangular shell finite elements, Finite Elem. Anal. Design 33 (1999) 83–124.
[16] G.M. Kulikov, S.V. Plotnikova, Comparative analysis of two algorithms for numerical solution of nonlinear static problems for multilayered anisotropic shells of revolution. 2. Account of transverse compression, Mech. Compos. Mater. 35 (1999) 293–300.
[17] G.M. Kulikov, Refined global approximation theory of multilayered plates and shells, J. Engrg. Mech. 127 (2001) 119–125.
[18] G.M. Kulikov, Analysis of initially stressed multilayered shells, Int. J. Solids Struct. 38 (2001) 4535–4555.
[19] G.M. Kulikov, S.V. Plotnikova, Simple and effective elements based upon Timoshenko–Mindlin shell theory, Comput. Meth. Appl. Mech. Engrg. 191 (2002) 1173–1187.
[20] G.M. Kulikov, S.V. Plotnikova, Mixed finite-element method for multilayered shells under localized loading. 1. Geometrically linear analysis, Mechanics of Composite Materials 38 (2002) 397–406.
[21] G.M. Kulikov, S.V. Plotnikova, Finite element formulation of straight composite beams undergoing finite rotations, Trans. Tambov State Technical University 7 (2001) 617–633.
[22] H. Parisch, A continuum-based shell theory for non-linear applications, Int. J. Numer. Meth. Engrg. 38 (1995) 1855–1883.
[23] H.C. Park, C. Cho, S.W. Lee, An efficient assumed strain element model with six DOF per node for geometrically non-linear shell, Int. J. Numer. Meth. Engrg. 38 (1995) 4101–4122.
[24] S. Klinkel, F. Gruttmann, W. Wagner, A continuum based three-dimensional shell element for laminated structures, Comput. Struct. 71 (1999) 43–62.
[25] C. Miehe, A theoretical and computational model for isotropic elastoplastic stress analysis in shells at large strains, Comput. Meth. Appl. Mech. Engrg. 155 (1998) 193–223.
[26] P. Betsch, F. Gruttmann, E. Stein, A 4-node finite shell element for the implementation of general hyperelastic 3D-elasticity at finite strains, Comput. Meth. Appl. Mech. Engrg. 130 (1996) 57–79.
[27] Y. Basar, M. Itskov, A. Eckstein, Composite laminates: nonlinear interlaminar stress analysis by multi-layer shell elements, Comput. Meth. Appl. Mech. Engrg. 185 (2000) 367–397.
[28] M. Bischoff, E. Ramm, On the physical significance of higher order kinematic and static variables in a three-dimensional shell formulation, Int. J. Solids Struct. 37 (2000) 6933–6960.
[29] T.J.R. Hughes, T.E. Tezduyar, Finite elements based upon Mindlin plate theory with particular reference to the four-node bilinear isoparametric element, Trans. ASME J. Appl. Mech. 48 (1981) 587–596.
[30] G. Wempner, D. Talaslidis, C.M. Hwang, A simple and efficient approximation of shells via finite quadrilateral elements, Trans. ASME J. Appl. Mech. 49 (1982) 115–120.
[31] K. Washizu, Variational Methods in Elasticity and Plasticity, third ed., Pergamon Press, Oxford, 1982.
[32] S.P. Timoshenko, On the correction for shear of the differential equation for transverse vibrations of prismatic bars, Philos. Mag. J. Sci. Ser. 6 41 (1921) 744–746.
[33] E.I. Grigolyuk, G.M. Kulikov, Multilayered Reinforced Shells: Analysis of Pneumatic Tires, Mashinostroyenie, Moscow, 1988 (in Russian).
[34] A.L. Gol'denveiser, Theory of Elastic Thin Shell, Pergamon Press, Oxford, 1961.
[35] G.M. Kulikov, Non-linear analysis of multilayered shells under initial stress, Int. J. Non-Linear Mech. 36 (2001) 323–334.
[36] T.J.R. Hughes, W.K. Liu, Nonlinear finite element analysis of shells. Part II. Two-dimensional shells, Comput. Meth. Appl. Mech. Engrg. 27 (1981) 167–182.
[37] D. Lam, W.K. Liu, E.S. Law, T. Belytschko, Resultant-stress degenerated-shell element, Comput. Meth. Appl. Mech. Engrg. 55 (1986) 259–300.

[38] K.J. Bathe, E.N. Dvorkin, A formulation of general shell elements—the use of mixed interpolation of tensorial components, Int. J. Numer. Meth. Engrg. 22 (1986) 697–722.
[39] J.C. Simo, D.D. Fox, M.S. Rifai, On a stress resultant geometrically exact shell model. Part II. The linear theory; computational aspects, Comput. Meth. Appl. Mech. Engrg. 73 (1989) 53–92.
[40] T. Belytschko, I. Leviathan, Physical stabilization of the 4-node shell element with one-point quadrature, Comput. Meth. Appl. Mech. Engrg. 113 (1994) 321–350.
[41] J.H. Argyris, M. Papadrakakis, C. Apostolopoulou, S. Koutsourelakis, The TRIC shell element: theoretical and numerical investigation, Comput. Meth. Appl. Mech. Engrg. 182 (2000) 217–245.
[42] K.J. Bathe, S. Bolourchi, Large displacement analysis in three-dimensional beam structures, Int. J. Numer. Meth. Engrg. 14 (1979) 961–986.
[43] J.C. Simo, L. Vu-Quoc, A three-dimensional finite strain rod model. Part II. Computational aspects, Comput. Meth. Appl. Mech. Engrg. 58 (1986) 79–116.
[44] A. Cardona, M. Geradin, A beam finite element non-linear theory with finite rotation, Int. J. Numer. Meth. Engrg. 26 (1988) 2403–2438.
[45] M.A. Crisfield, A consistent co-rotational formulation for non-linear three-dimensional beam elements, Comput. Meth. Appl. Mech. Engrg. 81 (1990) 131–150.
[46] L.A. Crivelli et al., A three-dimensional non-linear Timoshenko beam based on the core-congruental formulation, Int. J. Numer. Meth. Engrg. 36 (1993) 3647–3673.
[47] M. Li, The finite deformation theory for beam, plate and shell. Part III. The three-dimensional beam theory and the FE formulation, Comput. Meth. Appl. Mech. Engrg. 162 (1998) 287–300.
[48] F. Gruttmann, S. Klinkel, W. Wagner, A finite rotation shell theory with application to composite structures, Rev. Eur. Éléments finis 4 (1995) 597–631.
[49] C.H. Yeom, S.W. Lee, An assumed strain finite element model for large deflection composite shells, Int. J. Numer. Meth. Engrg. 28 (1989) 1749–1768.